Cell Reports

Article

BCL-XL inhibition induces an FGFR4-mediated rescue response in colorectal cancer

Graphical abstract

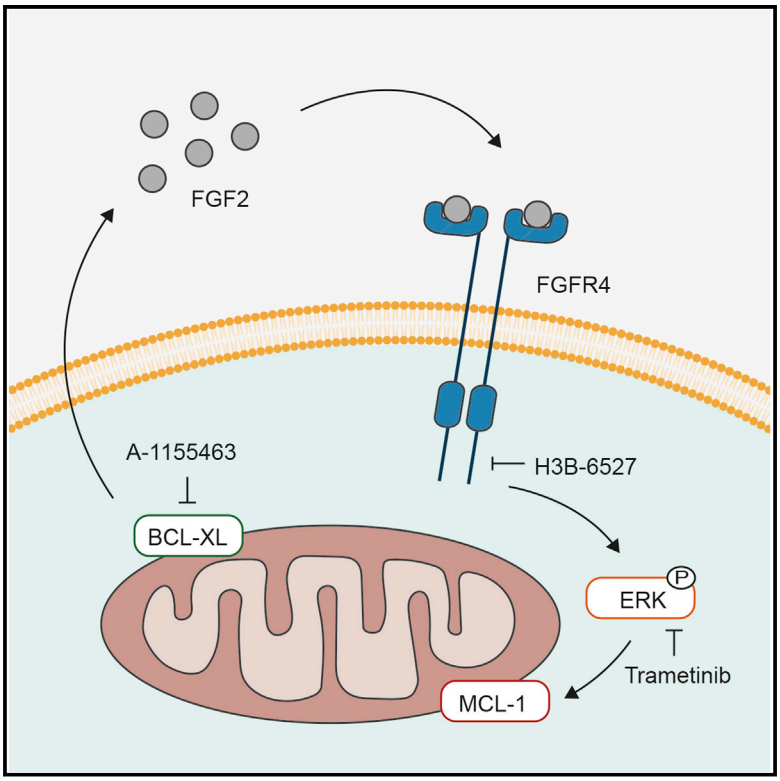

Authors

Prashanthi Ramesh, Simone Di Franco, Lidia Atencia Taboada, Le Zhang, Annalisa Nicotra, Giorgio Stassi, Jan Paul Medema

Correspondence

j.p.medema@amsterdamumc.nl

In brief

BCL-XL is crucial for apoptosis evasion in colorectal cancer and can be targeted with BH3 mimetics. Ramesh et al. screen a compound library to identify sensitizers of BH3 mimetic-induced apoptosis, which reveals a rescue response that involves rapid secretion of FGF2 upon BCL-XL inhibition and subsequent FGFR4 signaling-mediated MCL-1 upregulation.

Highlights

- FGFR4 inhibition sensitizes CRC cells to BCL-XL inhibition and spares normal cells
- BCL-XL targeting BH3 mimetics induce FGF2-mediated FGFR4 pathway activation
- FGFR4 activation in CRC cells can induce apoptosis resistance by upregulating MCL-1

Ramesh et al., 2022, Cell Reports *38*, 110374
February 15, 2022
https://doi.org/10.1016/j.celrep.2022.110374

CellPress

Cell Reports

CellPress
OPEN ACCESS

Article

BCL-XL inhibition induces an FGFR4-mediated rescue response in colorectal cancer

Prashanthi Ramesh,[1,2] Simone Di Franco,[3,4] Lidia Atencia Taboada,[1,2,4] Le Zhang,[1,2] Annalisa Nicotra,[3] Giorgio Stassi,[3] and Jan Paul Medema[1,2,5,*]

[1]Laboratory for Experimental Oncology and Radiobiology, Center for Experimental and Molecular Medicine, AmsterdamUMC, University of Amsterdam, Cancer Center Amsterdam, Meibergdreef 9, 1105 AZ Amsterdam, the Netherlands
[2]Oncode Institute, Meibergdreef 9, 1105 AZ Amsterdam, the Netherlands
[3]Department of Surgical Oncological and Stomatological Sciences, University of Palermo, Palermo, Italy
[4]These authors contributed equally
[5]Lead contact
*Correspondence: j.p.medema@amsterdamumc.nl
https://doi.org/10.1016/j.celrep.2022.110374

SUMMARY

The heterogeneous therapy response observed in colorectal cancer is in part due to cancer stem cells (CSCs) that resist chemotherapeutic insults. The anti-apoptotic protein BCL-XL plays a critical role in protecting CSCs from cell death, where its inhibition with high doses of BH3 mimetics can induce apoptosis. Here, we screen a compound library for synergy with low-dose BCL-XL inhibitor A-1155463 to identify pathways that regulate sensitivity to BCL-XL inhibition and reveal that fibroblast growth factor receptor (FGFR)4 inhibition effectively sensitizes to A-1155463 both *in vitro* and *in vivo*. Mechanistically, we identify a rescue response that is activated upon BCL-XL inhibition and leads to rapid FGF2 secretion and subsequent FGFR4-mediated post-translational stabilization of MCL-1. FGFR4 inhibition prevents MCL-1 upregulation and thereby sensitizes CSCs to BCL-XL inhibition. Altogether, our findings suggest a cell transferable induction of a FGF2/FGFR4 rescue response in CRC that is induced upon BCL-XL inhibition and leads to MCL-1 upregulation.

INTRODUCTION

Colorectal cancer (CRC) is a leading cause of cancer-related deaths worldwide (Bray et al., 2018). Effective treatment strategies have improved 5-year patient survival rates to approximately 90% for early-stage disease. However, despite intensive chemo- and targeted therapy, survival drops to as low as 5%–15% at advanced stages, particularly in the case of metastatic disease (Howlader et al., 2020).

Resistance to chemotherapy is in part driven by the intratumoral heterogeneity observed in CRC lesions (De Sousa et al., 2013). Most CRC tumors are hierarchically organized with cancer stem cells (CSCs) at the apex of this hierarchy. CSCs are a small subset of cells within the tumor population, with the ability to differentiate into multiple progeny and thereby drive tumor growth (Fessler et al., 2013). Importantly, our previous work suggests that the CSC population displays plasticity, in part regulated by the microenvironment (Vermeulen et al., 2010). Moreover, several studies have shown colon CSCs to be particularly resistant to chemotherapeutic insults, thereby enabling tumor repopulation (Colak et al., 2014; Dylla et al., 2008; Todaro et al., 2007). This resistance capacity is also enhanced by the microenvironment and calls for treatment strategies that enable eradication of this subpopulation to achieve efficient tumor remission (Colak and Medema, 2016).

Chemotherapy-induced stress results in the activation of the mitochondrial apoptosis pathway whereby upregulated pro-apoptotic BH3-only proteins overcome anti-apoptotic BCL-2 proteins and ultimately initiate caspase activity to execute cell death (Ramesh and Medema, 2020). Resistance to apoptosis by the upregulation of anti-apoptotic BCL-2 family proteins is frequently observed in several tumor types (Ni Chonghaile et al., 2011; Vo et al., 2012). Many hematological malignancies rely on BCL-2 for apoptosis evasion and are, therefore, sensitive to its specific inhibitor, ABT-199 (Venetoclax) (Valentin et al., 2018). In contrast, solid tumors seem to depend more on BCL-XL overexpression as a mechanism of anti-apoptotic adaptation (Amundson et al., 2000). Several studies have observed the upregulation of BCL-XL in CRC lesions and its inhibition with highly specific BH3 mimetics WEHI-539, A-1155463, and A-1331852 effectively targeting CRC cell lines and xenografts for cell death (Colak et al., 2014; Leverson et al., 2015a; Maurer et al., 1998; Tao et al., 2014; Zhang et al., 2015). In this regard, we have previously reported that colon CSCs in particular upregulate BCL-XL and are thereby less primed for mitochondrial cell death in comparison with their differentiated progeny (Colak et al., 2014). In agreement, we showed that targeting BCL-XL with high doses of WEHI-539 impairs CSC clonogenicity and sensitizes them to chemotherapy (Colak et al., 2014). More recently, we have shown that

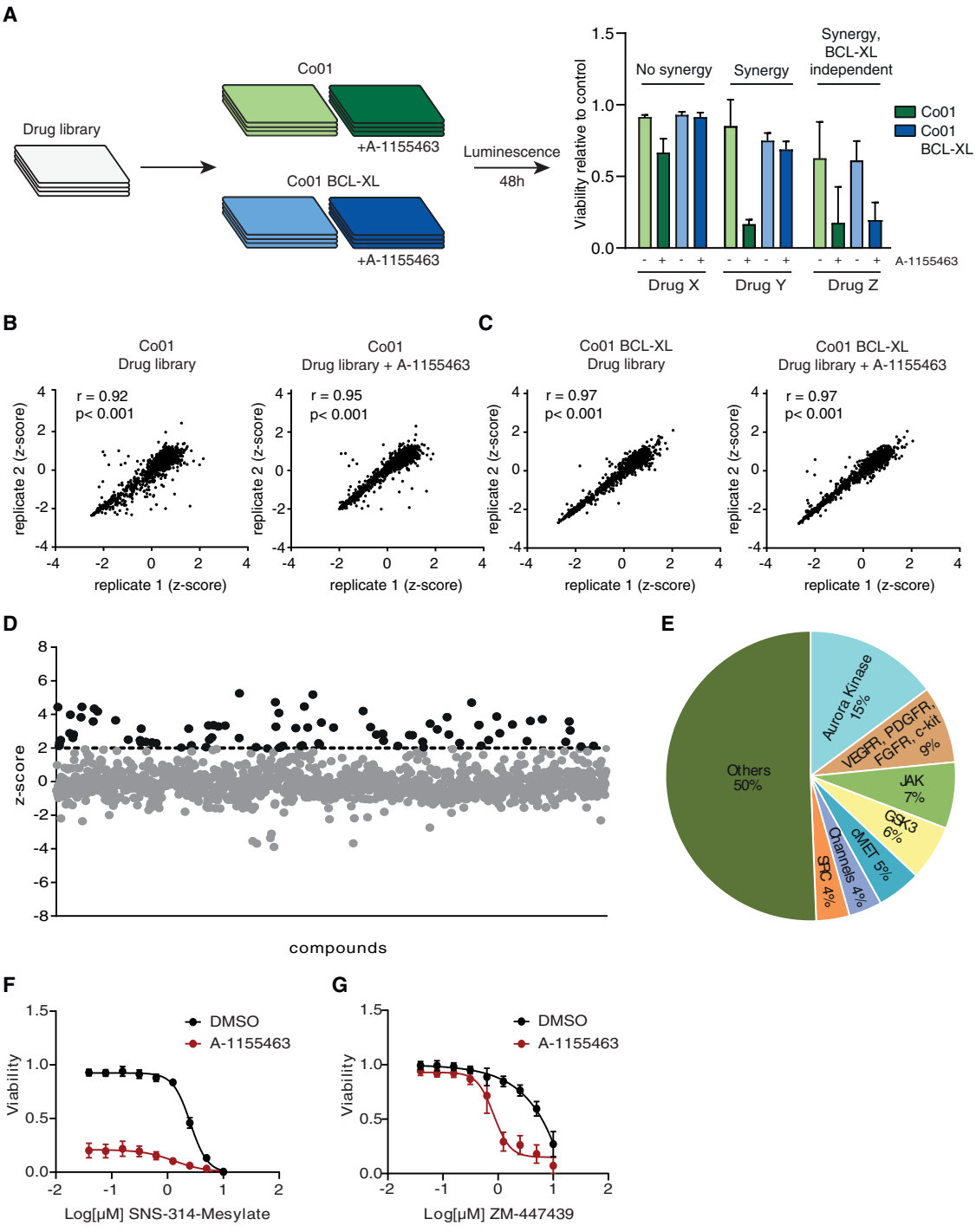

Figure 1. Drug screen identifies compounds that synergize with low-dose BCL-XL inhibition

(A) Schematic overview of the drug screen setup. Primary spheroid cultures Co01 and Co01 overexpressing BCL-XL were treated with 1402 inhibitors either alone or in combination with 5 nM A-1155463 and assayed for cell viability at 48 h. Compounds that induced strong cytotoxicity in combination with A-1155463 on Co01 but not Co01 BCL-XL were selected.

(B and C) Scatterplot of *Z* score normalized viability data of Co01 (B) and Co01 BCL-XL (C) treated with the library alone or in combination with A-1155463 (n = 1402). Plots show the correlation between two technical replicates and the data represent the *Z* score of each tested compound.

(D) *Z* score plot of the combination effect with A-1155463 for all inhibitors tested on Co01. Values represent the *Z* score-normalized average of two technical replicates. Hits were selected with a *Z* score cut-off of 2 or higher (dashed line).

(legend continued on next page)

BCL-XL plays a critical role in CRC initiation and progression, as targeting BCL-XL with the more potent BCL-XL antagonist A-1155463 significantly impaired clonogenic potential of adenoma and tumor organoids, while sparing normal colon organoids (Ramesh et al., 2021). While this would prove beneficial for CRC therapy, the clinical implementation of BCL-XL inhibition is hampered by the observed toxicity to platelets, whose lifespan is determined by BCL-XL expression (Schoenwaelder et al., 2011). We therefore designed a screen to elucidate signaling pathways that, when inhibited, synergize with targeting of BCL-XL in CSCs. Such synergistic effects not only provide mechanistic insight into CSC functioning, but can also be exploited as a therapeutic target minimizing toxic side effects.

Here we aimed to elucidate the pathways that can regulate BCL-XL dependency of colon CSCs; we screened compounds in combination with a low dose of the BCL-XL-specific inhibitor A-1155463 to identify hits that in combination facilitate cell death. We thus identified a group of receptor tyrosine kinase (RTK) inhibitors that strongly synergize with low-dose A-1155463 to target colon CSCs and patient-derived tumor organoids for apoptosis. Importantly, these inhibitors did not enhance BH3 mimetic-induced toxicity to healthy colon cells and platelets. Gene expression analysis and combinations with selective inhibitors revealed that the efficacy of the identified hits resulted from inhibition of fibroblast growth factor receptor (FGFR)4 signaling. Mechanistic insight indicated that cells treated with low-dose A-1155363 activate a rescue response by upregulating MCL-1. Furthermore, we find that such BCL-XL inhibition results in a rapid FGF2-mediated activation of FGFR4 signaling, which could mediate ERK-dependent MCL-1 stabilization by phosphorylation. Targeting FGFR4 could, therefore, prevent the activation of this rescue response and facilitate BH3 mimetic-induced cell death in CRC cells. Our findings suggest a rapid induction of resistance to anti-apoptotic protein inhibition, which occurs even in the absence of apoptosis and can be circumvented by concomitant inhibition of the FGFR4 signaling pathway.

RESULTS

Drug screen identifies compounds that synergize with low-dose BCL-XL inhibition

To identify compounds that interfere with pathways that regulate sensitivity toward BCL-XL inhibition and, thus, in effect lower the threshold of A-1155463-induced colon CSC apoptosis, we screened a primary colon spheroid culture Co01 with 1402 unique inhibitors alone and in combination with a low dose of A-1155463 (Figure 1A). A-1155463 was chosen for BCL-XL inhibition as it was significantly more potent in comparison with the previously used WEHI-539 (Figure S1A) (Tao et al., 2014). We defined the low dose of A-1155463 around the EC_{10} dose for this CRC line, wherein the drug did not induce significant cell death, but was starting to show impact on Co01, in order to maximize the potential to identify sensitizing agents. Based on the titration of A-1155463 on Co01 cells, we set the low dose at 5 nM with which we observed an average of 8% decrease in viability (Figure S1B). Of note, the sensitivity of A-1155463 on this primary cell line is with an EC_{50} of approximately 0.1μM, in the low range compared with earlier work where the EC_{50} values for CRC cell lines were reported to range from 0.035 to greater than 10 μM (Zhang et al., 2015). To validate that the chosen dose of A-1155463 was non-toxic to platelets, a known side effect of targeting BCL-XL *in vivo*, we performed a titration on platelets derived from human whole blood samples. Treatment for 2 h did not affect platelet viability, while after 6 h, only the higher doses resulted in platelet cell death. At 24 h, A-1155463 had a calculated EC_{50} of approximately 0.5 μM for human platelets, while there was no toxicity observed at 5 nM, thus confirming that 5 nM was a low, non-toxic dose *in vitro* for platelets (Figure S1C). As an additional control for the screen and to ensure that the inhibitors specifically overcome BCL-XL-driven resistance, we also screened all compounds on Co01 transduced with a BCL-XL overexpression plasmid. This line is more resistant to A-1155463 (approximately 10-fold) and inhibitors that also affected this line in combination with A-1155463 were not considered a true hit as they likely enhance cell death in a non-BCL-XL-dependent manner (Figures 1A and S1B).

The compound library included a range of small-molecule inhibitors targeting key signaling pathways, compounds and chemotherapeutics approved bu the US Food and Drug Administration (Table S1). Before the addition of drugs, cells were first allowed to proliferate overnight and subsequently treated for 2 days. after which cell viability was analyzed (Figure 1A; see STAR Methods). Viability data were *Z* score normalized and replicate measurements were highly correlated for both conditions with and without A-1155463, in both spheroid cultures tested (Figures 1B and 1C). To further ensure assay reliability, we calculated the median *Z* factor score across all screening plates and obtained a score of 0.73 (n = 128, upper quartile = 0.80, lower quartile = 0.66), indicating an experimentally robust assay.

In order to select hits from the screen, we calculated the added effect of each inhibitor in combination with A-1155463 in comparison with its effect alone and normalized the data by *Z* score (Table S1; see STAR Methods). Co01 targeting hits were selected with a *Z* score cut-off of 2 or higher (Figure 1D). Upon exclusion of compounds that also targeted the BCL-XL overexpressing line, a total of 81 hits were selected based on these parameters. The selected hits were grouped by their common protein targets to identify potential underlying pathways whose inhibition could sensitize colon CSCs for A-1155463-induced apoptosis (Figure 1E). This analysis revealed that a large

(E) Pie chart of the common targets of all hits selected. The number of inhibitors out of all selected hits that target the respective proteins are indicated in percentages.

(F and G) Dose-response curve of Co01 treated with a titration of SNS-314-mesylate (F) or ZM-447439 (G) either alone or in combination with 5 nM A-1155463 for 48 h. Viability data were blank corrected and normalized to controls. Data are represented as mean ± standard deviation (n = 3 independent experiments). See also Figure S1 and Table S1.

percentage of the hit compounds target Aurora kinases (15%) (Figure 1E). Importantly, our earlier work has established that Aurora kinases play a role in colon CSC tumorigenicity and chemoresistance (Cammareri et al., 2010). Moreover, the combination of Aurora kinase inhibitors with BCL-XL inhibition has been shown to be synergistic in CRC cell lines (Shah et al., 2010). We further validated this on Co01 cells and confirmed that Aurora kinase inhibitors dramatically impair cell viability in combination with low-dose A-1155463 (Figures 1F and 1G). The identification of this previously reported combination confirmed the effectiveness of our screen in detecting relevant targets.

Hits from the screen synergize with A-1155463 to induce potent cytotoxicity in colon CSCs and patient-derived tumor organoids

Besides Aurora kinase inhibitors, we observed a large fraction of hits targeting a family of RTKs, including vascular endothelial growth factor receptor (VEGFR), platelet-derived growth factor receptor (PDGFR), FGFR, and c-kit, with most inhibitors targeting multiple receptors (Figure 2A). We validated these inhibitors in a titration on Co01 cells in combination with A-1155463 and found the most consistent and potent efficacy with four of them, namely, Ki8751, axitinib, nintedanib, and golvatinib (Figures 2B and S2A–S2C). Moreover, we analyzed the combinatorial efficacy of these inhibitors with A-1155463 using the Bliss independence model, where scores or greater than 10 were considered indicative of synergy beyond additive effects. All four inhibitors showed synergy with A-1155463 over a range of concentrations (Figure 2C). Of the remaining hits in this group, CYC116 not only targets VEGFR, but is also a potent inhibitor of Aurora A/B and we, therefore, concluded that its observed efficacy could also result from Aurora kinase inhibition or a combination of the two (Figure S2A). CP-673451 and crenolanib, both of which are specific inhibitors of PDGFR, showed limited efficacy in a titration with A-1155463 (Figures S2B and S2C).

Earlier observations indicate that spheroid cultures represent a heterogeneous culture consisting of stem-like and differentiated populations that can be distinguished based on their Wnt activity, where Wnt-high colon CSCs exhibit enhanced BCL-XL-dependent chemotherapy resistance compared with more differentiated cancer cells (Colak et al., 2014; Vermeulen et al., 2010). We therefore assessed if the CSC population in the spheroid culture was effectively sensitized toward A-1155463-induced death by the identified hits. To do this, we took advantage of the Wnt reporter in Co01 cells (TOP-GFP) and measured cell death in the Wnt-high population by a fluorescence-activated cell sorting (FACS)-based assay that quantifies levels of activated caspase-3 at the single cell level. Single treatment with any of the inhibitors did not result in activation of caspase-3, while axitinib, Ki8751, and nintedanib significantly induced caspase-3 activity in CSC when combined with 5 nM A-1155463 (Figure 2D). Only the combination with golvatinib did not significantly target CSCs and therefore this drug was excluded from further experiments.

Next, to ensure that the selected combinations did not lead to sensitization of healthy colon-derived cells, we treated human normal colon organoids with all three inhibitors alone and in combination with A-1155463 and found that they were not sensitive to any of the inhibitors or the combinations (Figure 2E). In addition, we assessed the platelet toxicity of the combinations in human whole blood samples, where low-dose A-1155463 was also non-toxic in combination with any of the three inhibitors (Figure 2F).

To ascertain the clinical relevance of the observed sensitization, we extended our studies to include four primary patient-derived tumor organoids (p6T, p9T, p16T, and p24aT) (van de Wetering et al., 2015), which we treated in a 5 × 6 matrix titration with the selected inhibitors and A-1155463 (Figures 3A–3D, S3A–S3C). Synergy was analyzed at each dose combination with the Bliss independence model and positive scores were observed over a range of concentrations (Figures 3B–3D and S3A–S3C). To assess the overall efficacy of the combinations, we calculated the Bliss synergy scores for the most synergistic 3 × 3 dose window in the dose-response matrices. All inhibitors were synergistic in combination with A-1155463 across the four organoid cultures, except for Ki6751 in p6T and p16T (Figure 3E). Taken together, we identified and validated three potent inhibitors that synergize with a low dose of the BCL-XL inhibitor A-1155463 to induce CRC cell death, including the CSC population, while avoiding toxicity to healthy colon organoids and platelets.

FGFR4 inhibition potentiates A-1155463-mediated CSC cell death

The above validated inhibitors are known to target multiple RTKs and so, to identify the specific protein target responsible for the observed sensitization toward BCL-XL inhibition, we analyzed the mRNA expression profile of Co01 cells and found the highest expressed target to be *FGFR4*, followed by *FGFR3* (Figure 4A). Expression of FGFR4 in Co01 cells was also confirmed by flow cytometry (Figure S4A). The remaining targets including *VEGFR2* (*KDR*), *PDGFRa/b*, and *c-KIT* were all either lowly expressed or not expressed at all (Figure 4A). Moreover, selective PDGFR, c-KIT, or VEGFR inhibitors did not synergize with A-1155463, effectively excluding these receptors as potential targets (Figure S4B and Table S1). Analysis of gene expression data of the patient-derived tumor organoids revealed a similar pattern with *FGFR4* being the highest expressed target, followed by the remaining members of the *FGFR* family, while the other targets were detected at lower levels (Figure S4C).

To assess if FGFR4 inhibition mediates the observed synergy of the validated hits, we tested two FGFR4-specific inhibitors, BLU9931 and H3B-6527, and found that both significantly potentiated A-1155463-induced cytotoxicity (Figure S4D). In addition, the combination of FGFR4 inhibition with low-dose A-1155463 did not affect platelet viability *in vitro* (Figure S4E). Furthermore, both inhibitors enhanced A-1155463-mediated apoptosis in the TOP-GFP high CSC population, as measured by caspase-3 activation (Figure 4B), with a similar effect on the TOP-GFP low differentiated population (Figure S4F). Since other members of the FGFR family are also expressed in these cells, we tested an FGFR1/2/3 inhibitor, AZD4547, in a titration with A-1155463 and found no synergy between the two compounds (Figure S4G). Taken together, our data suggest that FGFR4 inhibition is required to achieve synergy with A-1155463-induced BCL-XL inhibition.

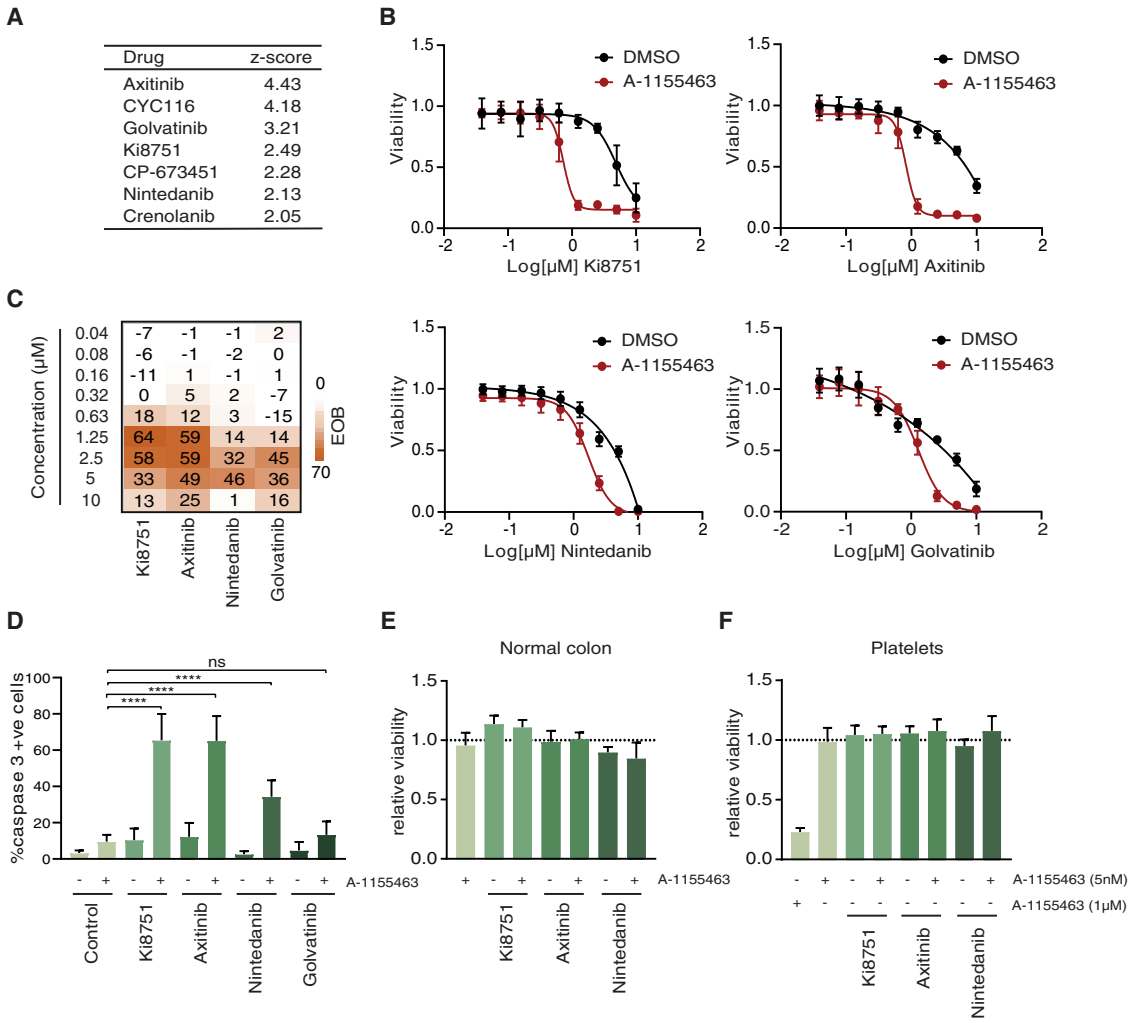

Figure 2. Selected hits induce CSC cell death in combination with A-1155463 while sparing normal colon organoids and platelets

(A) List of hit compounds that target several RTKs of the VEGFR, PDGFR, FGFR family, and c-kit along with their corresponding *Z* score from the screen.

(B) Dose-response curves of Co01 treated with a titration of Ki8751, axitinib, nintedanib, or golvatinib, alone and in combination with 5 nM A-1155463 for 48 h. Viability data were blank corrected and normalized to control. Data are represented as mean ± standard deviation (n = 3 independent experiments).

(C) Excess over bliss (EOB) synergy scores calculated for the dose-response data in (B).

(D) Percentage of activated caspase-3 in the 10% TOP-GFP high Co01 cells after 24 h treatment with 1 μM Ki8751, axitinib, nintedanib, or golvatinib, alone and in combination with 5 nM A-1155463. Data are represented as mean ± standard deviation (n = 3 independent experiments). ****p < 0.0001 (two-tailed unpaired Students *t* test).

(E) Normal colon organoids were treated with 1μM Ki8751, axitinib, or nintedanib, alone and in combination with 5 nM A-1155463 for 48 h, after which viability was measured. Data are plotted relative to control (dashed line) and represented as mean ± standard deviation (n = 3 independent experiments).

(F) Viability data of platelets derived from human whole blood treated with 1 μM Ki8751, axitinib, or nintedanib, alone and in combination with 5 nM A-1155463 for 24 h. Platelets were treated with 1 μM A-1155463 as a positive control for platelet toxicity. Data are plotted relative to control (dashed line) and represented as mean ± standard deviation (n = 3 independent experiments). See also Figure S2.

To assess whether FGFR4 inhibition is also crucial for sensitization of four distinct patient-derived tumor organoids, we treated these cells using a matrix titration of both BLU9931 and H3B-6527 in combination with A-1155463. We observed strong synergy as measured by the Bliss independence model at a range of dose combinations across all four organoid cultures (Figures 4C–4E, S5A and S5B). Finally, the combination of A-1155463 (1 mg/kg) and H3B-6527 (5 mg/kg) proved effective *in vivo* on subcutaneously injected Co01 tumors. At the end of the treatment, we found a significant delay in tumor outgrowth in the combination treatment group compared with the vehicle-treated mice, while the single treatments did not deter growth at this time point (Figure 4F). Previous studies have administered A-1155463 *in vivo* at a dose of 5 mg/kg, which was found to induce platelet toxicity (de Jong et al., 2018; Tao et al., 2014). We confirmed this in a platelet toxicity assay, where a single injection of 5 mg/kg and 25 mg/kg of A-1155463 resulted in significant platelet loss *in vivo* within 6 h with only minor recovery at

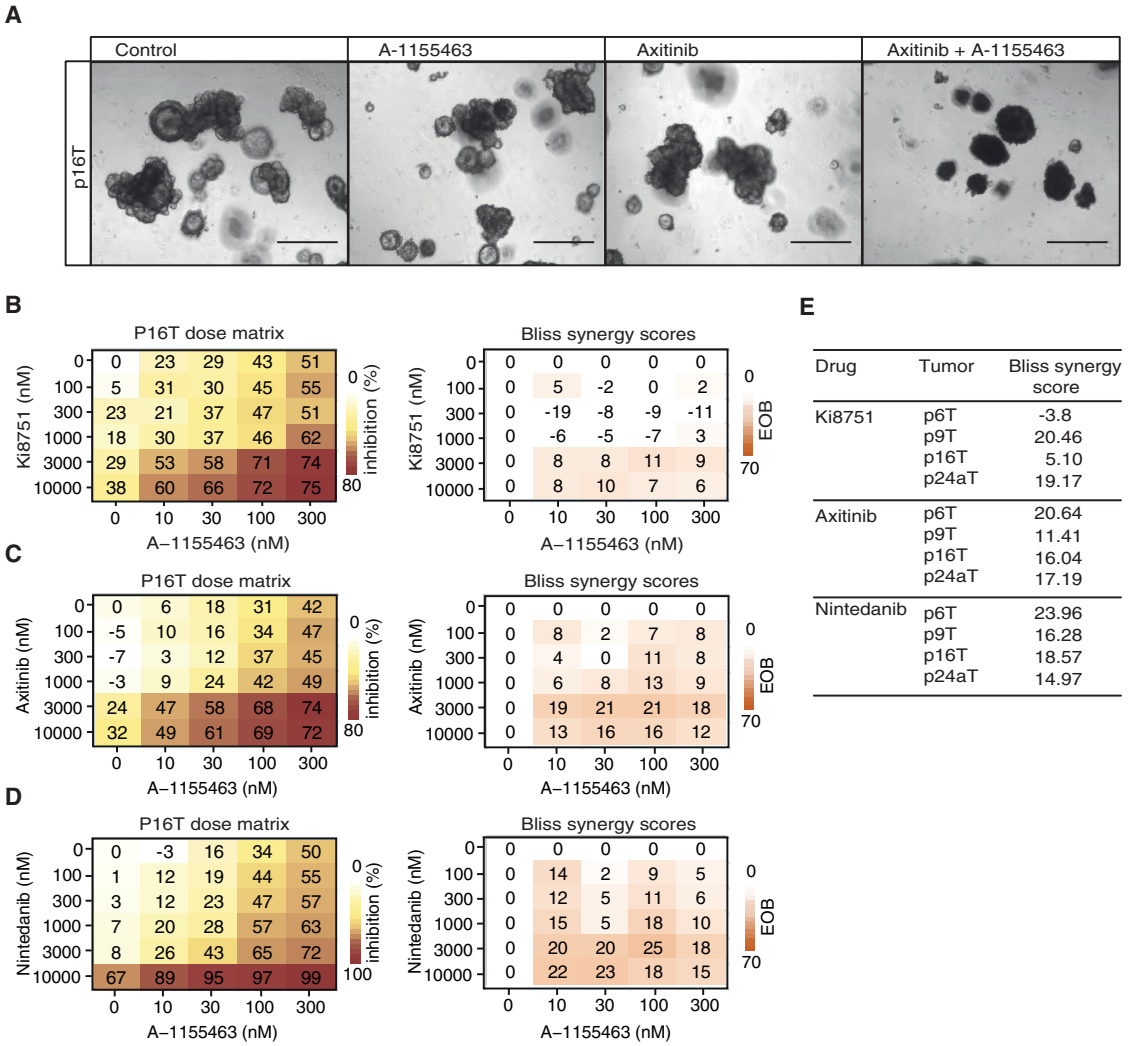

E

Drug	Tumor	Bliss synergy score
Ki8751	p6T	-3.8
	p9T	20.46
	p16T	5.10
	p24aT	19.17
Axitinib	p6T	20.64
	p9T	11.41
	p16T	16.04
	p24aT	17.19
Nintedanib	p6T	23.96
	p9T	16.28
	p16T	18.57
	p24aT	14.97

Figure 3. Ki8751, axitinib, and nintedanib in combination with A-1155463 induce synergistic cytotoxicity in patient-derived tumor organoids

(A) Phase-contrast images of p16T human CRC organoids treated for 48 h with 10 μM axitinib alone and in combination with 30 nM A-1155463. Scale bars indicate 250 μm.

(B–D) The 5 × 6 dose matrices of P16T human CRC organoids treated with Ki8751 (B), axitinib (C), and nintedanib (D) in combination with A-1155463 for 48 h. The percent inhibition was calculated from viability data, after normalizing to control. Data represent the average of three independent experiments. Bliss synergy scores were calculated for each dose combination.

(E) Human CRC organoids were treated in a 5 × 6 dose-response matrix with Ki8751, axitinib. and nintedanib in combination with A-1155463 for 48 h (n = 3 independent experiments). The Bliss synergy scores for the most synergistic 3 × 3 dose window in the dose-response matrices are listed in the table for each organoid and drug. See also Figure S3.

24 h for the 25 mg/kg dose (Figure S6A), while 1 mg/kg had no significant impact on platelet counts at the time points analyzed. Moreover, in the tumor growth experiment where mice were treated with the lower dose of 1 mg/kg, no discernable impact on platelet counts were observed during the course of the experiment either when applied alone or in combination with H3B-6527 (Figures 4G and S6A). Similarly, body weight measurements remained stable in all conditions throughout the treatment period (Figure S6B), suggesting that the combination therapy did not induce substantial (intestinal) toxicity. Altogether, our data provide evidence for improving BH3 mimetic efficacy in CRC with combined inhibition of FGFR4 signaling with a decrease in toxicity that is associated with high doses of BCL-XL targeting inhibitors.

BCL-XL inhibition induces an FGFR4-mediated rescue response

As we aimed to identify pathways regulating BCL-XL-dependent cell death, we next wanted to determine the underlying mechanism by which FGFR4 inhibition sensitizes tumor cells to A-1155463. First, we assessed the expression of anti-apoptotic proteins and found that FGFR4 inhibition with H3B-6527 in Co01 cells slightly lowered the expression of MCL-1 protein levels as quickly as 4 h after treatment, while BCL-XL levels

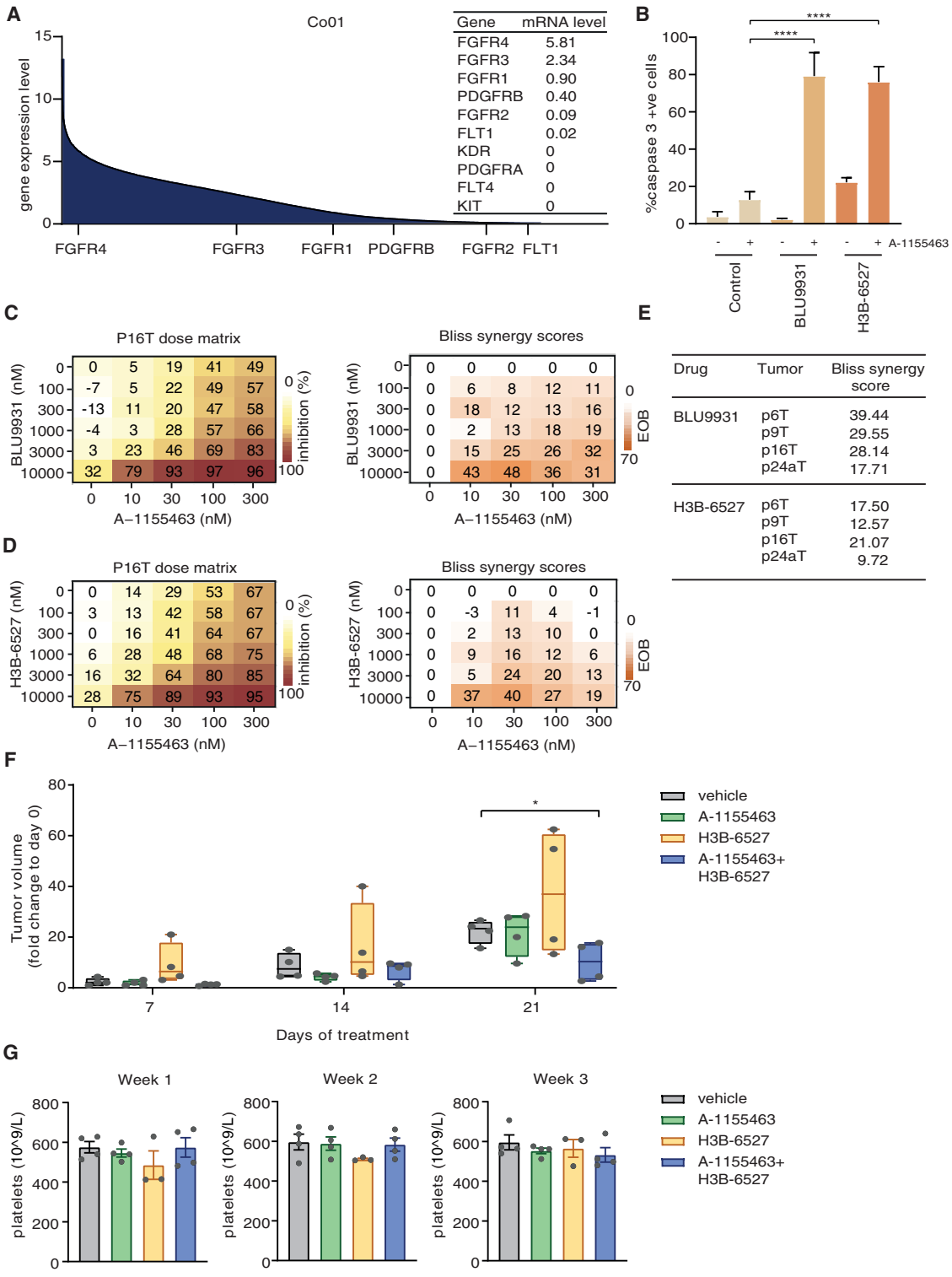

Figure 4. FGFR4 inhibition potentiates A-1155463-mediated CSC cell death

(A) mRNA expression profile of Co01 cells ranked by the Log2 expression level of the genes, ranging from 13 (highest) to 0 (lowest/undetected). The expression of known targets of Ki8751, axitinib, and nintedanib together are indicated.

(B) Percentage of activated caspase-3 in the 10% TOP-GFP high Co01 cells after 24 h treatment with 5 μM BLU9931 or H3B-6527, alone and in combination with 5 nM A-1155463. Data are represented as mean ± standard deviation (n = 3 independent experiments). ****p < 0.0001 (two-tailed unpaired Student *t* test).

(legend continued on next page)

remained unchanged (Figure 5A). Treatment with Ki8751, axitinib, and nintedanib induced a similar decrease in MCL-1 levels (Figure S7A). More important, this analysis revealed an unexpected induction of MCL-1 protein levels when cells were treated with 5 nM A-1155463 (Figure 5A). This suggests that low doses of BH3 mimetics trigger a cellular response that results in MCL-1 upregulation, which seems to qualify as a rescue response that is induced upon BCL-XL engagement. Moreover, our data indicate that this response involves FGFR4 as the combination with FGFR4 inhibitors prevents MCL-1 upregulation (Figure 5A) and seems to be regulated post-translationally, as no increase in *MCL1* mRNA was observed upon A-1155463 treatment (Figure S7B). Intriguingly, low-dose A-1155463 also induced FGFR4 phosphorylation, suggesting activation of the signaling pathway (Figure 5B). In addition, we observed a rapid phosphorylation of ERK, but not of AKT, upon treatment with A-1155463, which was also reduced by FGFR4 inhibition (Figure 5C). To further confirm the specificity of the inhibitors and assess if FGFR4 plays a role in the observed rescue response, we performed an shRNA-mediated knockdown of FGFR4 gene expression and found that A-1155463 induced MCL-1 upregulation was strongly reduced (Figures 5D and S7C).

ERK-mediated phosphorylation of the MCL-1-PEST domain has been reported to limit MCL-1 degradation. Our data therefore suggest that the induction of MCL-1 protein upon A-1155463 treatment could be mediated by FGFR4-driven ERK signaling (Domina et al., 2004) (Figure 5C). In support of this, we also observed an increase in the phosphorylation of MCL-1 upon A-1155463 treatment (Figure S7D). Although our observations suggest that FGFR4 activation leads to MCL-1 stabilization, alternative mechanisms for BH3 mimetic treatment-induced MCL-1 upregulation can still be at play. For instance, BCL-XL engagement with BH3 mimetics could induce MCL-1 stabilization by lowering NOXA binding to MCL-1, which would decrease MCL-1 proteasomal degradation. This could be achieved when BH3-only proteins are released from BCL-XL due to the treatment with A-1155463 and compete with NOXA for binding to MCL-1, hence leading to MCL-1 stabilization upon BH3 mimetic treatment (Kotschy et al., 2016; Leverson et al., 2015b; Tron et al., 2018). To assess if this is involved in upregulation of MCL-1, we made use of HCT-116 cells that are devoid of all pro-apoptotic BH3-only proteins (HCT-116 OctaKO), which are highly resistant to BCL-XL inhibition (O'Neill et al., 2016). Here, with increasing doses of A-1155463, a clear induction of MCL-1 was still observed (Figure 5E), where this effect was also FGFR4 dependent as H3B-6527 treatment prevented MCL-1 upregulation (Figure S7E). Although this excludes a role for BH3-only proteins in MCL-1 stabilization and the induction of the rescue response, we cannot formally rule out that changed interaction due to displacement of other players, such as BAX or BAK, from BCL-XL upon A-1155463 treatment contributes to MCL-1 stabilization.

It is important to note that both the screen and the validation experiments are performed in standard culture medium, which contains FGF2 to facilitate the growth of colon CSCs and A-1155463 could thus act by facilitating FGF2-FGFR4 signaling. However, even in the absence of exogenously added FGF2, we still observed FGFR4-dependent induction of MCL-1 upon treatment with A-1155463 (Figure S7G). This suggests that low-dose BCL-XL inhibition leads to FGFR4 signaling, which then induces MCL-1 upregulation. In agreement, combined treatment with H3B-6527 and A-1155463 also impaired the viability of Co01 cells in the absence of exogenously added FGF2 (Figure S7F). We therefore assessed if cells treated with low-dose A-1155463 could activate the FGFR4 pathway in a paracrine manner by transferring media from A-1155463-treated cells (Figure 5F). Strikingly, also supernatant of A-1155463-treated Co01 cells induced expression of MCL-1 in both HCT116 and SW948 recipient cells (Figures 5G and S7H). This MCL-1 induction was prevented when H3B-6527 was added to the supernatant to prevent FGFR4 activation (Figures 5G and S7H). Importantly, FGFR4 inhibition showed a significant but not complete prevention of MCL-1 upregulation, suggesting that other receptors may be activated as well by factors in the supernatant and transmit MCL-1 upregulation. Strong inhibition was also observed in both HCT116 and SW948 receiver cells upon the addition of trametinib, confirming a role for the ERK pathway in mediating the rescue response (Figures 5H and S7I). To address if ligand-driven activation of FGFR4 is responsible for this rescue response, we treated HCT116 and SW948 cells with FGF2, which also resulted in increased MCL-1 protein levels (Figures 5I and S7J). More important, the knockdown of FGF2 blocked the upregulation of MCL-1 upon A-1155463 treatment, suggesting that FGF2 could act as a potential transferable link between BCL-XL inhibition and MCL-1 upregulation (Figures 5J and S7K). Combined, our data point to a rapid upregulation of MCL-1 upon A-1155463 treatment that is likely due to the activation of a rescue response by release of FGF2, activation of FGFR4, and the subsequent ERK-dependent phosphorylation and stabilization of MCL-1.

To further confirm that the observed induction of MCL-1 expression is indeed responsible for the resistance of colon CSCs to BCL-XL targeting, we tested the sensitivity of Co01 cells to combined BCL-XL and MCL-1 inhibition. Treatment with the MCL-1 inhibitor AZD-5991 is capable of inducing apoptosis in Co01, but only at very high doses. In combination with

(C and D) The 5 × 6 dose matrices of P16T human CRC organoids treated with BLU9931 (C) and H3B-6527 (D) in combination with A-1155463 for 48 h. The percent inhibition was calculated from viability data, after normalizing to control. Data represent the average of three independent experiments. Bliss synergy scores were calculated for each dose combination.

(E) Human CRC organoids were treated in a 5 × 6 dose response matrix with BLU9931 and H3B-6527 in combination with A-1155463 for 48 h (n = 3 independent experiments). The Bliss synergy scores for the most synergistic 3 × 3 dose window in the dose-response matrices are listed in the table for each organoid and drug.

(F) Boxplot of the volume of Co01 subcutaneous tumors on days 7, 14, and 21 compared with day 0. Mice were treated with vehicle, H3B-6527, A-1155463, or a combination (n = 4 mice per group). *$p < 0.05$ (two-tailed unpaired Student *t* test).

(G) Platelet counts determined from the tail vein blood of mice treated with vehicle, H3B-6527, A-1155463, or a combination, counted at the end of each week of treatment for three weeks (n = 4 mice per group). Data are represented as mean ± standard error of the mean. See also Figures S4, S5, and S6.

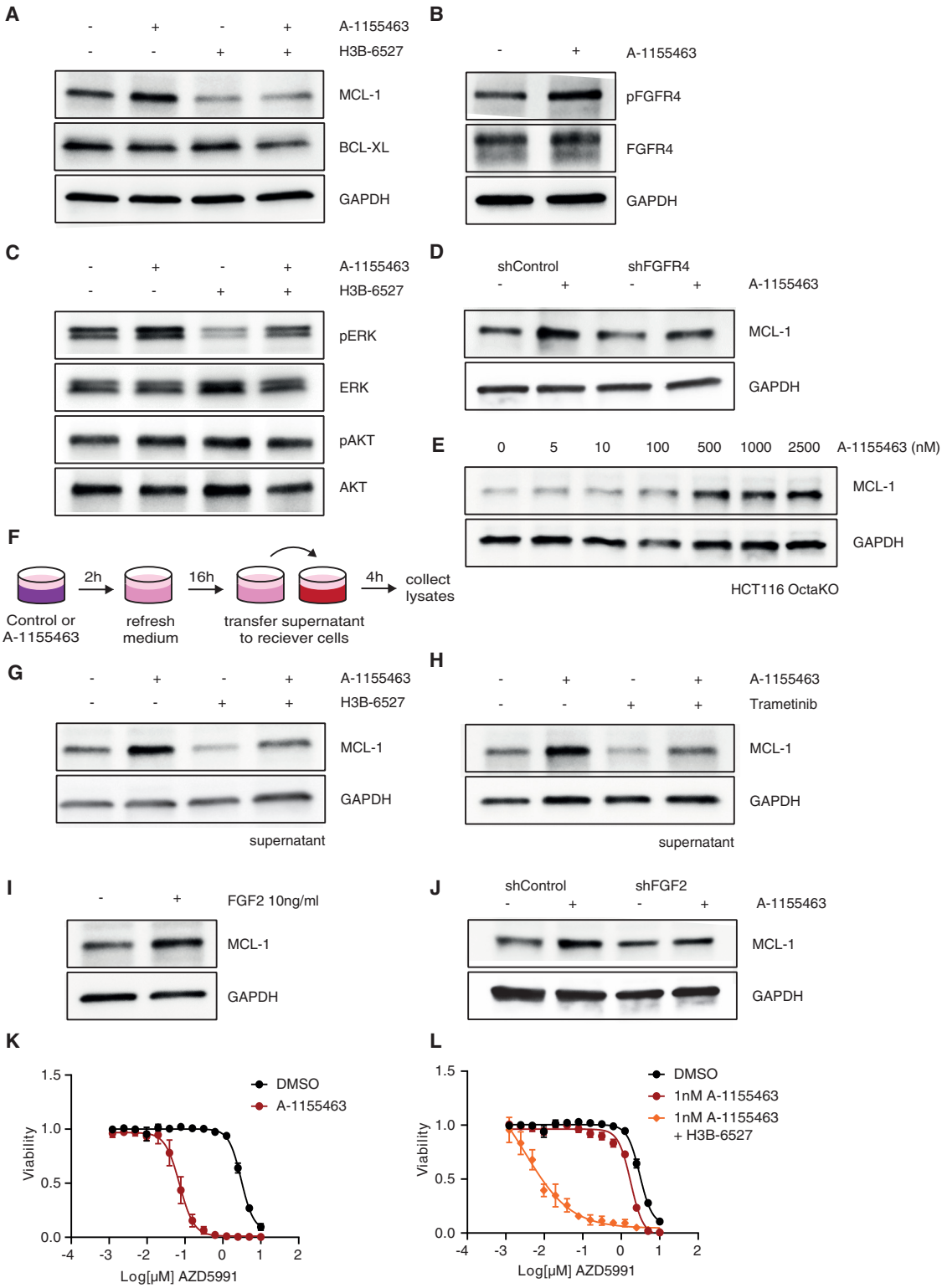

Figure 5. BCL-XL inhibition induces an FGFR4-mediated rescue response

(A) Immunoblot analysis of MCL-1 and BCL-XL levels in Co01 cells treated with 5 nM A-1155463, 5 μM H3B-6527, or a combination of the two for 4 h. GAPDH was used as a loading control.

(B) Immunoblot analysis of pFGFR4 and FGFR4 levels in Co01 cells treated with 5 nM A-1155463 for 1 h, without bFGF in the culture medium. GAPDH was used as a loading control.

(legend continued on next page)

low-dose A-1155463 a potent (approximately 50 fold) shift in the EC_{50} was observed (Figure 5K). This confirms a strong synergy between BCL-XL and MCL-1 inhibition, similar to earlier reports (Berger et al., 2016; Greaves et al., 2019; Soderquist et al., 2018), suggesting that decreasing MCL-1 levels by FGFR4 inhibition could act in a similar manner and facilitate A-1155463-induced apoptosis as well. To test this, we hypothesized that lowering MCL-1 expression through FGFR4 inhibition should lower the dose of AZD-5991 needed to completely block MCL-1 and allow low-dose A-1155463 to achieve complete cell death. We, therefore, treated cells with a less effective dose combination of H3B-6527 and A-1155463, to which part of the Co01 cells were still resistant, allowing further analysis of MCL-1 targeting efficiency (Figures S7I and S7L). Upon correcting for the basal apoptosis induced by this combination, we assessed the efficacy of AZD-5991 in inducing apoptosis in the presence of H3B-6527 and A-1155463 and observed a very significant shift toward lower AZD-5991 concentration needed to kill the cells (Figure 5L). Altogether, our data point to an FGFR4-dependent rescue response that is activated upon low-dose BCL-XL inhibition to induce MCL-1 upregulation. The inhibition of this pathway, therefore, lowers the anti-apoptotic threshold and enhances cell death induced by BCL-XL targeting drugs.

DISCUSSION

Our understanding of stem cell functionality in CRC has advanced remarkably with help from studies that highlight the dynamic nature of this population (De Sousa et al., 2017; Shimokawa et al., 2017). Indeed, several intrinsic and extrinsic cues can induce de-differentiation of tumor cells to model more stem-like characteristics with associated therapy resistance (Colak and Medema, 2016; Prasetyanti and Medema, 2017). Considering the malleability of this population, it is pertinent to identify therapeutic strategies that either target the microenvironmental signals or the cell-intrinsic pathways that govern CSC clonogenicity and resistance (Vermeulen et al., 2012). In this regard, we have previously identified BCL-XL as a key mediator of CRC stem cell therapy resistance, making it a relevant target for eradicating not only CSCs but also differentiated cells with the potential to revert to more stem-like states (Colak et al., 2014).

Here, using a screen set-up, we identified and validated FGFR4 as a synergistic target for BCL-XL inhibition in several CRC models. More important, our data identify a rescue response that is induced when cells are treated with A-1155463, which results in MCL-1 upregulation. Importantly, this stimulation is relatively rapid and not due to enhanced transcription, as mRNA levels of MCL-1 were unchanged. Our data would propose the regulation of MCL-1 protein stability through ERK-dependent phosphorylation, which is induced by FGFR4 pathway activation upon A-1155463 treatment.

The identified FGFR4-mediated rescue pathway could be exploited to sensitize cancer cells to A-1155463 as shown by the absence of toxicity of the combination therapy in normal intestinal cells and platelets, both *in vitro* and *in vivo*. This likely results from the fact that normal intestinal epithelial cells are resistant to BCL-XL inhibition (Ramesh et al., 2021; van der Heijden et al., 2016). Moreover, FGFR4 expression is absent in the intestinal epithelium, while it is upregulated in CRC tumors (Liu et al., 2013; Stark et al., 1991; Turkington et al., 2014). However, in our *in vivo* model, FGFR4 inhibition on its own leads to variable effects with some tumors showing increased growth upon H3B-6527 treatment. This is in contrast with the *in vitro* effects of H3B-6527 on Co01 cells, where FGFR4 inhibition does induce low levels of apoptosis. This suggests that blocking FGFR4 *in vivo* may have some additional non-tumor-cell-related effects. Potentially, this relates to an effect on stromal cells, which could affect tumor growth indirectly, but the underlying mechanisms need further exploration.

Currently, several clinical trials are ongoing testing selective FGFR4 inhibition mainly in hepatocellular carcinoma, but also including other $FGFR4^+$ advanced solid tumors (Clinicaltrials.gov) (Mercade et al., 2019; Weiss et al., 2019). Our data suggest that a combination with apoptosis inducing drugs could benefit the therapeutic efficacy of FGFR4 inhibition. This observation is not limited to CRC; studies in other solid tumor types report similar synergy between BH3 mimetics and FGFR pathway

(C) Immunoblot analysis of pERK, ERK, pAKT, and AKT levels in Co01 cells treated with 5 nM A-1155463, 5 μM H3B-6527, or a combination of the two for 4 h. GAPDH was used as a loading control.
(D) Immunoblot analysis of MCL-1 levels in Co01 cells with either a control (shControl) or FGFR4 knockdown (shFGFR4) treated with 5nM A-1155463 for 4h. GAPDH was used as a loading control.
(E) Immunoblot analysis of MCL-1 levels in HCT116 OctaKO cells, depleted of all BH3 only proteins, treated with indicated doses of A-1155463 for 4 h. GAPDH was used as a loading control.
(F) Schematic overview of the supernatant transfer experiment. Co01 cells were cultured with or without 5 nM A115 for 2 h, after which the medium was refreshed. Supernatants were collected after 16 h and transferred to recipient cells for 4 h before analysis.
(G) Immunoblot analysis of MCL-1 levels in HCT116 cells that received supernatant of control or 5 nM A-1155463 conditioned cells as described in (F), in the presence or absence of 5 μM H3B-6527 for 4 h. GAPDH was used as a loading control.
(H) Immunoblot analysis of MCL-1 levels in HCT116 cells that received supernatant of control or 5 nM A-1155463-conditioned cells as described in (F), in the presence or absence of 5 μM trametinib for 4 h. GAPDH was used as a loading control.
(I) Immunoblot analysis of MCL-1 levels in HCT116 cells treated with 10 ng/mL FGF2 for 4 h. GAPDH was used as a loading control.
(J) Immunoblot analysis of MCL-1 levels in HCT116 cells with either a control (shControl) or FGF2 knockdown (shFGF2) treated with 5 nM A-1155463 for 4 h. GAPDH was used as a loading control.
(K) Dose-response curve of Co01 treated with a titration of MCL-1 inhibitor AZD5991 alone and in combination with 5 nM A-1155463 for 48 h. Viability data were blank corrected and normalized to control. Data are represented as mean ± standard deviation (n = 3 independent experiments).
(L) Dose-response curve of Co01 treated with a titration of MCL-1 inhibitor AZD5991 alone and in combination with 1 nM A-1155463 and 5 μM H3B-6527 for 48 h. Viability data were blank corrected and normalized to control. Data are represented as mean ± standard deviation (n = 3 independent experiments).
All immunoblots represent one of two independent experiments with similar results. See also Figure S7.

inhibition (Packer et al., 2019; Turunen et al., 2019; Weeden et al., 2018). In breast cancer cells, A-1155463 was found to significantly potentiate BLU9931-induced cell death in a study examining the role of FGFR4-mediated resistance, indicating broader applicability of this combination strategy in solid tumors (Turunen et al., 2019).

Importantly, our data suggest that treatment with BH3 mimetics alone might not be fully clinically effective, giving rise to rapid MCL-1-driven resistance. In agreement, treatment with a low dose of A-1155463 is ineffective in impairing tumor growth. This is further supported by our recent findings, where we used tamoxifen to induce transformation in the mouse colon and treated with A-1155463 either during transformation or after transformation (Ramesh et al., 2021). Interestingly, we found that BCL-XL inhibition is effective in preventing adenoma formation, but once the adenomas are fully formed, A-1155463 treatment on its own no longer deters the adenoma growth rate. Potentially also in this setting, the combined inhibition of BCL-XL with FGFR4 or MCL-1 inhibition presents a strategy that could overcome this resistance mechanism.

Recent data indicate that the role of MCL-1 in the intestine is complex (Healy et al., 2020), where its deletion resulted in aberrant cell death under homeostatic conditions. However, over time MCL-1-deficient crypts presented with increased proliferation and expansion of the stem cell compartment, indicative of a compensatory regenerative mechanism (Healy et al., 2020). Proliferation was dependent on Wnt signaling and eventually resulted in adenoma formation, indicating that the deletion or targeting of MCL-1 may have detrimental side effects in the intestine by enhancing compensatory proliferation and carcinogenesis.

Whether this apoptosis-associated proliferation relates to the response we observe in CRC cells treated with low-dose BH3 mimetics is not clear, but is an intriguing possibility. In MCL-1-deficient mice, extensive cell death results in a loss of integrity of the epithelial lining and has a significant impact on the epithelial barrier function of the intestine (Healy et al., 2020). To resolve this loss, a rapid regeneration is required to avoid a hyper-inflammatory response. A signal emanating from dying cells to alert surroundings cells to start a compensatory proliferative response could be a physiologically relevant response to damage. In this light, it is interesting to note that a similar regenerative response follows upon extensive cell death when the intestine is exposed to irradiation or during inflammatory conditions such as inflammatory bowel disease. In the case of irradiation-induced apoptosis, both PUMA and NOXA, two BH3 molecules induced by p53 activation, are reportedly essential (Qiu et al., 2008; Shibue et al., 2003). We speculate that in this setting BH3 molecules in dying cells could instruct surrounding cells to become resistant and start dividing to preserve barrier function. Intriguingly, a role for FGF signaling in this regenerative process has been extensively described. For instance, FGF2 is quickly induced upon irradiation and provides a survival benefit for epithelial cells (Houchen et al., 1999). Rescue induced by FGF family members could, therefore, be a more general mechanism in the intestinal epithelium that is hijacked by CRC cells. Indeed, our data suggest that the deletion of FGF2 blocks the upregulation of MCL-1, in support of this hypothesis. However, this does not exclude that different FGFs can mediate this response, possibly also through different FGF receptors, depending on tissue- and disease-specific settings. The near complete inhibition of MCL-1 induction by blocking FGFR4 in HCT116 cells (Figure 5G) suggests that FGFR4 is important, but may not be unique. It seems, however, that FGF2 is crucial for the effect, but how treatment with BH3 mimetics translates to a signal for FGF2 release is a mechanism that needs further exploration.

In this study, we observe that BCL-XL inhibition relays an FGF2 driven signal that can be transferred with conditioned media, where this signal is activated quite rapidly upon low-dose BH3 mimetic treatment. This suggests that cell death induction is not a prerequisite for the observed effect. However, whether only cells that are bound for cell death due to increased apoptotic priming release this rescue signal requires further analysis. Nevertheless, we conclude that combining low doses of BCL-XL targeting BH3 mimetics with FGFR4 inhibition provides a non-toxic therapeutic opportunity to target CRC cells, including the more resistant CSC population. More important, this combination largely prevents the rapidly induced resistance mechanism observed upon BCL-XL inhibition alone, thus providing a rationale to improve BH3 mimetic efficacy in the treatment of solid tumors.

Limitations of the study

Our observations strongly suggest that BCL-XL inhibition results in the FGFR4-mediated upregulation of MCL-1. However, it cannot be ruled out that the observed increase in MCL-1 levels upon A-1155463 treatment might also arise from FGFR-independent effects, such as the displacement of BAX/BAK from BCL-XL to MCL-1, leading to its stabilization by the displacement of NOXA or MULE. Furthermore, our study highlights a potential therapeutic opportunity for combined inhibition of FGFR4 and BCL-XL in CRC. While our *in vivo* experiment supports this, it is limited in numbers and does not induce dramatic reduction in tumor growth rate upon combination treatment. More extensive *in vivo* testing of this treatment strategy would be required to solidify its therapeutic benefit in CRC clinical management.

STAR★METHODS

Detailed methods are provided in the online version of this paper and include the following:

- KEY RESOURCES TABLE
- RESOURCE AVAILABILITY
  - Lead contact
  - Materials availability
  - Data and code availability
- EXPERIMENTAL MODEL AND SUBJECT DETAILS
  - Spheroid cultures
  - Organoid cultures
  - Cell lines
  - Mice for platelet toxicity assay
- MICE FOR TUMOR GROWTH ASSAY
- METHOD DETAILS
  - Compounds
  - Drug screen workflow

- Viability assays
- Flow cytometry assisted cell sorting
- *Ex vivo* platelet toxicity
- Platelet counting from tail vein bleeds
- *In vivo* drug treatment
- RNA sequencing and data analysis
- Quantitative real-time PCR
- Supernatant transfer
- Immunoblotting

● QUANTIFICATION AND STATISTICAL ANALYSES

- Screen data analysis
- Bliss synergy score

SUPPLEMENTAL INFORMATION

Supplemental information can be found online at https://doi.org/10.1016/j.celrep.2022.110374.

ACKNOWLEDGMENTS

Supported by Oncode, KWF project 2015–7587 and 10150. L.Z. was supported by a CSC scholarship. G.S. is supported by AIRC 5x1000 #9979, AIRC IG 21445, and PRIN 2017WNKSLR grants. The authors would like to thank the laboratory of Xu Luo at the University of Nebraska Medical Center for kindly providing the HCT116 OctaKO cell line. The authors would also like to thank Ferry de Klein for assistance with the drug dispensing robot.

AUTHOR CONTRIBUTIONS

Conception and design of the study: P.R. and J.P.M. Experimental work: P.R., S.F., L.A.T., L.Z., and A.N. Data analysis and interpretation: P.R., S.F., and J.P.M. Drafting of the manuscript: P.R, J.P.M. Final manuscript contribution: P.R., S.F., L.A.T., L.Z., A.N., G.S., and J.P.M.

DECLARATION OF INTERESTS

J.P.M. serves as an advisor to AbbVie on their colorectal cancer program. All other authors declare no potential competing interests.

Received: March 23, 2021
Revised: September 27, 2021
Accepted: January 21, 2022
Published: February 15, 2022

REFERENCES

Amundson, S.A., Myers, T.G., Scudiero, D., Kitada, S., Reed, J.C., and Fornace, A.J., Jr. (2000). An informatics approach identifying markers of chemosensitivity in human cancer cell lines. Cancer Res. *60*, 6101–6110.

Berger, S., Procko, E., Margineantu, D., Lee, E.F., Shen, B.W., Zelter, A., Silva, D.A., Chawla, K., Herold, M.J., Garnier, J.M., et al. (2016). Computationally designed high specificity inhibitors delineate the roles of BCL2 family proteins in cancer. Elife *5*, e20352. https://doi.org/10.7554/eLife.20352.

Bray, F., Ferlay, J., Soerjomataram, I., Siegel, R.L., Torre, L.A., and Jemal, A. (2018). Global cancer statistics 2018: GLOBOCAN estimates of incidence and mortality worldwide for 36 cancers in 185 countries. CA Cancer J. Clin. *68*, 394–424. https://doi.org/10.3322/caac.21492.

Buikhuisen, J.Y., Gomez Barila, P.M., Torang, A., Dekker, D., de Jong, J.H., Cameron, K., Vitale, S., Stassi, G., van Hooff, S.R., Castro, M.A.A., et al. (2021). AKT3 expression in mesenchymal colorectal cancer cells drives growth and is associated with epithelial-mesenchymal transition. Cancers (Basel) *13*, 801. https://doi.org/10.3390/cancers13040801.

Cammareri, P., Scopelliti, A., Todaro, M., Eterno, V., Francescangeli, F., Moyer, M.P., Agrusa, A., Dieli, F., Zeuner, A., and Stassi, G. (2010). Aurora-a is essential for the tumorigenic capacity and chemoresistance of colorectal cancer stem cells. Cancer Res. *70*, 4655–4665. https://doi.org/10.1158/0008-5472.Can-09-3953.

Colak, S., and Medema, J.P. (2016). Human colonic fibroblasts regulate stemness and chemotherapy resistance of colon cancer stem cells. Cell Cycle *15*, 1531–1537. https://doi.org/10.4161/15384101.2014.973321.

Colak, S., Zimberlin, C.D., Fessler, E., Hogdal, L., Prasetyanti, P.R., Grandela, C.M., Letai, A., and Medema, J.P. (2014). Decreased mitochondrial priming determines chemoresistance of colon cancer stem cells. Cell Death Differ. *21*, 1170–1177. https://doi.org/10.1038/cdd.2014.37.

de Jong, Y., Monderer, D., Brandinelli, E., Monchanin, M., van den Akker, B.E., van Oosterwijk, J.G., Blay, J.Y., Dutour, A., and Bovée, J. (2018). Bcl-xl as the most promising Bcl-2 family member in targeted treatment of chondrosarcoma. Oncogenesis *7*, 74. https://doi.org/10.1038/s41389-018-0084-0.

De Sousa, E.M.F., Kurtova, A.V., Harnoss, J.M., Kljavin, N., Hoeck, J.D., Hung, J., Anderson, J.E., Storm, E.E., Modrusan, Z., Koeppen, H., et al. (2017). A distinct role for Lgr5(+) stem cells in primary and metastatic colon cancer. Nature *543*, 676–680. https://doi.org/10.1038/nature21713.

De Sousa, E.M.F., Vermeulen, L., Fessler, E., and Medema, J.P. (2013). Cancer heterogeneity–a multifaceted view. EMBO Rep. *14*, 686–695. https://doi.org/10.1038/embor.2013.92.

Domina, A.M., Vrana, J.A., Gregory, M.A., Hann, S.R., and Craig, R.W. (2004). MCL1 is phosphorylated in the PEST region and stabilized upon ERK activation in viable cells, and at additional sites with cytotoxic okadaic acid or taxol. Oncogene *23*, 5301–5315. https://doi.org/10.1038/sj.onc.1207692.

Dylla, S.J., Beviglia, L., Park, I.K., Chartier, C., Raval, J., Ngan, L., Pickell, K., Aguilar, J., Lazetic, S., Smith-Berdan, S., et al. (2008). Colorectal cancer stem cells are enriched in xenogeneic tumors following chemotherapy. PLoS One *3*, e2428. https://doi.org/10.1371/journal.pone.0002428.

Fessler, E., Dijkgraaf, F.E., De Sousa, E.M.F., and Medema, J.P. (2013). Cancer stem cell dynamics in tumor progression and metastasis: is the microenvironment to blame? Cancer Lett. *341*, 97–104. https://doi.org/10.1016/j.canlet.2012.10.015.

Greaves, G., Milani, M., Butterworth, M., Carter, R.J., Byrne, D.P., Eyers, P.A., Luo, X., Cohen, G.M., and Varadarajan, S. (2019). BH3-only proteins are dispensable for apoptosis induced by pharmacological inhibition of both MCL-1 and BCL-X(L). Cell Death Differ. *26*, 1037–1047. https://doi.org/10.1038/s41418-018-0183-7.

Healy, M.E., Boege, Y., Hodder, M.C., Böhm, F., Malehmir, M., Scherr, A.L., Jetzer, J., Chan, L.K., Parrotta, R., Jacobs, K., et al. (2020). MCL1 is required for maintenance of intestinal homeostasis and prevention of carcinogenesis in mice. Gastroenterology *159*, 183–199. https://doi.org/10.1053/j.gastro.2020.03.017.

Houchen, C.W., George, R.J., Sturmoski, M.A., and Cohn, S.M. (1999). FGF-2 enhances intestinal stem cell survival and its expression is induced after radiation injury. Am. J. Physiol. *276*, G249–G258. https://doi.org/10.1152/ajpgi.1999.276.1.G249.

N. Howlader, A.M. Noone, M. Krapcho, D. Miller, A. Brest, M. Yu, J. Ruhl, Z. Tatalovich, A. Mariotto, D.R. Lewis, H.S. Chen, E.J. Feuer, and K.A. Cronin, eds. (2020). SEER Cancer Statistics Review, 1975 - 2017, National Cancer Institute. Bethesda, MD (Based on November 2019 SEER data submission, posted to the SEER web site, April 2020). https://seer.cancer.gov/csr/1975_2017/.

Ianevski, A., He, L., Aittokallio, T., and Tang, J. (2017). SynergyFinder: a web application for analyzing drug combination dose-response matrix data. Bioinformatics *33*, 2413–2415. https://doi.org/10.1093/bioinformatics/btx162.

Kotschy, A., Szlavik, Z., Murray, J., Davidson, J., Maragno, A.L., Le Toumelin-Braizat, G., Chanrion, M., Kelly, G.L., Gong, J.N., Moujalled, D.M., et al. (2016). The MCL1 inhibitor S63845 is tolerable and effective in diverse cancer models. Nature *538*, 477–482. https://doi.org/10.1038/nature19830.

Leverson, J.D., Phillips, D.C., Mitten, M.J., Boghaert, E.R., Diaz, D., Tahir, S.K., Belmont, L.D., Nimmer, P., Xiao, Y., Ma, X.M., et al. (2015a). Exploiting selective BCL-2 family inhibitors to dissect cell survival dependencies and define

improved strategies for cancer therapy. Sci. Transl. Med. *7*, 279ra240. https://doi.org/10.1126/scitranslmed.aaa4642.

Leverson, J.D., Zhang, H., Chen, J., Tahir, S.K., Phillips, D.C., Xue, J., Nimmer, P., Jin, S., Smith, M., Xiao, Y., et al. (2015b). Potent and selective small-molecule MCL-1 inhibitors demonstrate on-target cancer cell killing activity as single agents and in combination with ABT-263 (navitoclax). Cell Death Dis. *6*, e1590. https://doi.org/10.1038/cddis.2014.561.

Liu, R., Li, J., Xie, K., Zhang, T., Lei, Y., Chen, Y., Zhang, L., Huang, K., Wang, K., Wu, H., et al. (2013). FGFR4 promotes stroma-induced epithelial-to-mesenchymal transition in colorectal cancer. Cancer Res. *73*, 5926–5935. https://doi.org/10.1158/0008-5472.Can-12-4718.

Maurer, C.A., Friess, H., Bühler, S.S., Wahl, B.R., Graber, H., Zimmermann, A., and Büchler, M.W. (1998). Apoptosis inhibiting factor Bcl-xL might be the crucial member of the Bcl-2 gene family in colorectal cancer. Dig. Dis. Sci. *43*, 2641–2648. https://doi.org/10.1023/a:1026695025990.

Mercade, T.M., Moreno, V., John, B., Morris, J.C., Sawyer, M.B., Yong, W.P., Gutierrez, M., Karasic, T.B., Sangro, B., Sheng-Shun, Y., et al. (2019). A phase I study of H3B-6527 in hepatocellular carcinoma (HCC) or intrahepatic cholangiocarcinoma (ICC) patients (pts). J. Clin. Oncol. *37*, 4095. https://doi.org/10.1200/JCO.2019.37.15_suppl.4095.

Ni Chonghaile, T., Sarosiek, K.A., Vo, T.T., Ryan, J.A., Tammareddi, A., Moore Vdel, G., Deng, J., Anderson, K.C., Richardson, P., Tai, Y.T., et al. (2011). Pretreatment mitochondrial priming correlates with clinical response to cytotoxic chemotherapy. Science *334*, 1129–1133. https://doi.org/10.1126/science.1206727.

O'Neill, K.L., Huang, K., Zhang, J., Chen, Y., and Luo, X. (2016). Inactivation of prosurvival Bcl-2 proteins activates Bax/Bak through the outer mitochondrial membrane. Genes Dev. *30*, 973–988. https://doi.org/10.1101/gad.276725.115.

Packer, L.M., Stehbens, S.J., Bonazzi, V.F., Gunter, J.H., Ju, R.J., Ward, M., Gartside, M.G., Byron, S.A., and Pollock, P.M. (2019). Bcl-2 inhibitors enhance FGFR inhibitor-induced mitochondrial-dependent cell death in FGFR2-mutant endometrial cancer. Mol. Oncol. *13*, 738–756. https://doi.org/10.1002/1878-0261.12422.

Prasetyanti, P.R., and Medema, J.P. (2017). Intra-tumor heterogeneity from a cancer stem cell perspective. Mol. Cancer *16*, 41. https://doi.org/10.1186/s12943-017-0600-4.

Qiu, W., Carson-Walter, E.B., Liu, H., Epperly, M., Greenberger, J.S., Zambetti, G.P., Zhang, L., and Yu, J. (2008). PUMA regulates intestinal progenitor cell radiosensitivity and gastrointestinal syndrome. Cell Stem Cell *2*, 576–583. https://doi.org/10.1016/j.stem.2008.03.009.

Ramesh, P., Lannagan, T.R.M., Jackstadt, R., Atencia Taboada, L., Lansu, N., Wirapati, P., van Hooff, S.R., Dekker, D., Pritchard, J., Kirov, A.B., et al. (2021). BCL-XL is crucial for progression through the adenoma-to-carcinoma sequence of colorectal cancer. Cell Death Differ. *28*, 3282–3296. https://doi.org/10.1038/s41418-021-00816-w.

Ramesh, P., and Medema, J.P. (2020). BCL-2 family deregulation in colorectal cancer: potential for BH3 mimetics in therapy. Apoptosis *25*, 305–320. https://doi.org/10.1007/s10495-020-01601-9.

Sato, T., Stange, D.E., Ferrante, M., Vries, R.G., Van Es, J.H., Van den Brink, S., Van Houdt, W.J., Pronk, A., Van Gorp, J., Siersema, P.D., and Clevers, H. (2011). Long-term expansion of epithelial organoids from human colon, adenoma, adenocarcinoma, and Barrett's epithelium. Gastroenterology *141*, 1762–1772. https://doi.org/10.1053/j.gastro.2011.07.050.

Schoenwaelder, S.M., Jarman, K.E., Gardiner, E.E., Hua, M., Qiao, J., White, M.J., Josefsson, E.C., Alwis, I., Ono, A., Willcox, A., et al. (2011). Bcl-xL-inhibitory BH3 mimetics can induce a transient thrombocytopathy that undermines the hemostatic function of platelets. Blood *118*, 1663–1674. https://doi.org/10.1182/blood-2011-04-347849.

Shah, O.J., Lin, X., Li, L., Huang, X., Li, J., Anderson, M.G., Tang, H., Rodriguez, L.E., Warder, S.E., McLoughlin, S., et al. (2010). Bcl-XL represents a druggable molecular vulnerability during aurora B inhibitor-mediated polyploidization. Proc. Natl. Acad. Sci. U. S. A. *107*, 12634–12639. https://doi.org/10.1073/pnas.0913615107.

Shibue, T., Takeda, K., Oda, E., Tanaka, H., Murasawa, H., Takaoka, A., Morishita, Y., Akira, S., Taniguchi, T., and Tanaka, N. (2003). Integral role of Noxa in p53-mediated apoptotic response. Genes Dev. *17*, 2233–2238. https://doi.org/10.1101/gad.1103603.

Shimokawa, M., Ohta, Y., Nishikori, S., Matano, M., Takano, A., Fujii, M., Date, S., Sugimoto, S., Kanai, T., and Sato, T. (2017). Visualization and targeting of LGR5(+) human colon cancer stem cells. Nature *545*, 187–192. https://doi.org/10.1038/nature22081.

Soderquist, R.S., Crawford, L., Liu, E., Lu, M., Agarwal, A., Anderson, G.R., Lin, K.H., Winter, P.S., Cakir, M., and Wood, K.C. (2018). Systematic mapping of BCL-2 gene dependencies in cancer reveals molecular determinants of BH3 mimetic sensitivity. Nat. Commun. *9*, 3513. https://doi.org/10.1038/s41467-018-05815-z.

Stark, K.L., McMahon, J.A., and McMahon, A.P. (1991). FGFR-4, a new member of the fibroblast growth factor receptor family, expressed in the definitive endoderm and skeletal muscle lineages of the mouse. Development *113*, 641–651.

Tao, Z.F., Hasvold, L., Wang, L., Wang, X., Petros, A.M., Park, C.H., Boghaert, E.R., Catron, N.D., Chen, J., Colman, P.M., et al. (2014). Discovery of a potent and selective BCL-XL inhibitor with in vivo activity. ACS Med. Chem. Lett. *5*, 1088–1093. https://doi.org/10.1021/ml5001867.

Todaro, M., Alea, M.P., Di Stefano, A.B., Cammareri, P., Vermeulen, L., Iovino, F., Tripodo, C., Russo, A., Gulotta, G., Medema, J.P., and Stassi, G. (2007). Colon cancer stem cells dictate tumor growth and resist cell death by production of interleukin-4. Cell Stem Cell *1*, 389–402. https://doi.org/10.1016/j.stem.2007.08.001.

Tron, A.E., Belmonte, M.A., Adam, A., Aquila, B.M., Boise, L.H., Chiarparin, E., Cidado, J., Embrey, K.J., Gangl, E., Gibbons, F.D., et al. (2018). Discovery of Mcl-1-specific inhibitor AZD5991 and preclinical activity in multiple myeloma and acute myeloid leukemia. Nat. Commun. *9*, 5341. https://doi.org/10.1038/s41467-018-07551-w.

Turkington, R.C., Longley, D.B., Allen, W.L., Stevenson, L., McLaughlin, K., Dunne, P.D., Blayney, J.K., Salto-Tellez, M., Van Schaeybroeck, S., and Johnston, P.G. (2014). Fibroblast growth factor receptor 4 (FGFR4): a targetable regulator of drug resistance in colorectal cancer. Cell Death Dis. *5*, e1046. https://doi.org/10.1038/cddis.2014.10.

Turunen, S.P., von Nandelstadh, P., Öhman, T., Gucciardo, E., Seashore-Ludlow, B., Martins, B., Rantanen, V., Li, H., Höpfner, K., Östling, P., et al. (2019). FGFR4 phosphorylates MST1 to confer breast cancer cells resistance to MST1/2-dependent apoptosis. Cell Death Differ. *26*, 2577–2593. https://doi.org/10.1038/s41418-019-0321-x.

Valentin, R., Grabow, S., and Davids, M.S. (2018). The rise of apoptosis: targeting apoptosis in hematologic malignancies. Blood *132*, 1248–1264. https://doi.org/10.1182/blood-2018-02-791350.

van de Wetering, M., Francies, H.E., Francis, J.M., Bounova, G., Iorio, F., Pronk, A., van Houdt, W., van Gorp, J., Taylor-Weiner, A., Kester, L., et al. (2015). Prospective derivation of a living organoid biobank of colorectal cancer patients. Cell *161*, 933–945. https://doi.org/10.1016/j.cell.2015.03.053.

van der Heijden, M., Zimberlin, C.D., Nicholson, A.M., Colak, S., Kemp, R., Meijer, S.L., Medema, J.P., Greten, F.R., Jansen, M., Winton, D.J., and Vermeulen, L. (2016). Bcl-2 is a critical mediator of intestinal transformation. Nat. Commun. *7*, 10916. https://doi.org/10.1038/ncomms10916.

Vermeulen, L., de Sousa e Melo, F., Richel, D.J., and Medema, J.P. (2012). The developing cancer stem-cell model: clinical challenges and opportunities. Lancet Oncol. *13*, e83–e89. https://doi.org/10.1016/s1470-2045(11)70257-1.

Vermeulen, L., De Sousa, E.M.F., van der Heijden, M., Cameron, K., de Jong, J.H., Borovski, T., Tuynman, J.B., Todaro, M., Merz, C., Rodermond, H., et al. (2010). Wnt activity defines colon cancer stem cells and is regulated by the microenvironment. Nat. Cell Biol. *12*, 468–476. https://doi.org/10.1038/ncb2048.

Vo, T.T., Ryan, J., Carrasco, R., Neuberg, D., Rossi, D.J., Stone, R.M., Deangelo, D.J., Frattini, M.G., and Letai, A. (2012). Relative mitochondrial priming of myeloblasts and normal HSCs determines chemotherapeutic success in AML. Cell *151*, 344–355. https://doi.org/10.1016/j.cell.2012.08.038.

Weeden, C.E., Ah-Cann, C., Holik, A.Z., Pasquet, J., Garnier, J.M., Merino, D., Lessene, G., and Asselin-Labat, M.L. (2018). Dual inhibition of BCL-XL and MCL-1 is required to induce tumour regression in lung squamous cell carcinomas sensitive to FGFR inhibition. Oncogene *37*, 4475–4488. https://doi.org/10.1038/s41388-018-0268-2.

Weiss, A., Adler, F., Buhles, A., Stamm, C., Fairhurst, R.A., Kiffe, M., Sterker, D., Centeleghe, M., Wartmann, M., Kinyamu-Akunda, J., et al. (2019). FGF401, A first-in-class highly selective and potent FGFR4 inhibitor for the treatment of FGF19-driven hepatocellular cancer. Mol. Cancer Ther. *18*, 2194–2206. https://doi.org/10.1158/1535-7163.Mct-18-1291.

Zhang, H., Xue, J., Hessler, P., Tahir, S.K., Chen, J., Jin, S., Souers, A.J., Leverson, J.D., and Lam, L.T. (2015). Genomic analysis and selective small molecule inhibition identifies BCL-X(L) as a critical survival factor in a subset of colorectal cancer. Mol. Cancer *14*, 126. https://doi.org/10.1186/s12943-015-0397-y.

Zhang, J.H., Chung, T.D., and Oldenburg, K.R. (1999). A simple statistical parameter for use in evaluation and validation of high throughput screening assays. J. Biomol. Screen *4*, 67–73. https://doi.org/10.1177/108705719900400206.

STAR★METHODS

KEY RESOURCES TABLE

REAGENT or RESOURCE	SOURCE	IDENTIFIER
Antibodies		
Rabbit polyclonal anti-MCL1	Cell Signaling Technology	Cat# 4572; RRID: AB_2281980
Rabbit monoclonal anti-BCL-XL (54H6)	Cell Signaling Technology	Cat# 2764; RRID: AB_2228008
Goat polyclonal Anti-Rabbit IgG(H+L), Mouse/Human ads-HRP	Southern Biotech	Cat# 4050-05; RRID: AB_2795955
Goat polyclonal Anti-Mouse IgG(H+L), Human ads-HRP	Southern Biotech	Cat# 1031-05; RRID: AB_2794307
Mouse monoclonal anti-GAPDH, clone 6C5	Sigma-Aldrich	Cat# MAB374; RRID: AB_2107445
Rabbit polyclonal Phospho-FGFR4 (Tyr642)	Thermo Fisher	Cat# PA5-37576; RRID: AB_2554184
Rabbit monoclonal FGF Receptor 4 (D3B12) XP	Cell Signaling Technology	Cat# 8562; RRID: AB_10891199
Rabbit polyclonal Phospho-p44/42 MAPK (Erk1/2) (Thr202/Tyr204)	Cell Signaling Technology	Cat# 9101; RRID: AB_331772
Mouse monoclonal p44/42 MAPK (Erk1/2) (3A7)	Cell Signaling Technology	Cat# 9107; RRID: AB_10695739
Rabbit monoclonal Phospho-Akt (Ser473) (D9E) XP	Cell Signaling Technology	Cat# 4060; RRID: AB_2224726
Rabbit polyclonal anti-AKT	Cell Signaling Technology	Cat# 9272; RRID: AB_329827
Rabbit monoclonal Phospho-Mcl-1 (Thr163) (D5M9D)	Cell Signaling Technology	Cat# 14765; RRID: AB_2716686
Mouse monoclonal PE anti-human CD334 (FGFR4), clone 4FR6D3	BioLegend	Cat# 324306; RRID: AB_2231698
Bacterial and virus strains		
Lentiviral construct pHEFTIR-BCL-XL	Colak et al., 2014	DOI: 10.1038/cdd.2014.37
TCF/LEF reporter TOP-GFP	Vermeulen et al., 2010	DOI: 10.1038/ncb2048
Biological samples		
Patient derived tumor organoids P6T, P9T, P16T and P24aT	van de Wetering et al., 2015	DOI: 10.1016/j.cell.2015.03.053
Normal colon organoids	Ramesh et al., 2021	DOI: 10.1038/s41418-021-00816-w
Chemicals, peptides, and recombinant proteins		
A-1155463	Chemietek	Cat# CT-A115
H3B-6527	Selleck Chemicals	Cat# S8675
Trametinib	Selleck Chemicals	Cat# S4484
L1100 Drug library	Selleck Chemicals	N/A
Puromycin	InvivoGen	Cat# ant-pr-1
RED-DEVD-FMK, CaspGLOW Red	BioVision	Cat# K193-25
Halt™ Protease Inhibitor Cocktail, EDTA-Free (100X)	Thermo Fisher Scientific	Cat# 87785
Matrigel Matrix	Corning	Cat# 354234
TrypLE Express Enzyme (1X), phenol red	Thermo Fischer Scientific	Cat# 12605010
SuperScript III reverse transcriptase	Thermo Fischer Scientific	Cat# 18080044
SYBR green master mix	Roche	Cat# 04887352001
RIPA Extraction and Lysis buffer	Thermo Fischer Scientific	Cat# 89900
LumiLight western blotting substrate	Sigma-Aldrich	Cat# 12015200001
DMSO	Sigma-Aldrich	Cat# 67-68-5

(*Continued on next page*)

Continued

REAGENT or RESOURCE	SOURCE	IDENTIFIER
PEG400	Sigma-Aldrich	Cat# 25322-68-3
Tween-80	Sigma-Aldrich	Cat# 9005-65-6
Ammonium Oxalate	Sigma-Aldrich	Cat# 6009-70-7
Critical commercial assays		
Pierce BCA Protein Assay Kit	Thermo Fisher Scientific	Cat# 23225
Nucleospin RNA isolation kit	Bioke	Cat# 740955.10
CellTiter-Blue® Cell Viability Assay	Promega	Cat# G8080
Trans-Blot Turbo transfer kit	Bio-Rad	Cat# 1704270
Deposited data		
Co01 RNA-seq expression profile	This paper	GEO: GSE159504
Tumor organoids RNA-seq expression profile	Van der Wetering et al., 2015	GEO: GSE64392
Experimental models: Cell lines		
Human: HCT116	Sanger Institute (Cambridge, United Kingdom)	N/A
Human: OctaKO HCT116	O'Neill et al., 2016	DOI:10.1101/gad.276725.115
Human: SW948	Sanger Institute (Cambridge, United Kingdom)	N/A
Human: colon cancer spheroid culture Co01	Vermeulen et al., 2010	DOI: 10.1038/ncb2048
Experimental models: Organisms/strains		
NSG® Mice (JAX® Mice Strain) NOD.Cg-Prkdcscid Il2rgtm1Wjl/SzJ	Charles River Laboratories	Cat# 614
NOD SCID (JAX® Mice Strain) NOD.CB17-Prkdcscid/J	Charles River Laboratories	Cat# 634
Oligonucleotides		
FGFR4 Forward: GGAGGAGCCAGGTGAGGA	This paper	N/A
FGFR4 Reverse: CAGGGCTCAAGCTCCACTTC	This paper	N/A
FGF2 Forward: TACAACTTCAAGCAGAAGAG	This paper	N/A
FGF2 Reverse: CAGCTCTTAGCAGACATTGG	This paper	N/A
RPLP0 Forward: GGCACCATTGAAATCCTGAGTGATGTG	This paper	N/A
RPLP0 Reverse: TTGCGGACACCCTCCAGGAAGC	This paper	N/A
Recombinant DNA		
pLKO.1-puro control shRNA, Mission shRNA	Merck	Cat# shc002
pLKO.1-puro FGFR4 shRNA, Mission shRNA	Merck	Cat# TRCN0000010531
pLKO.1-puro FGF2 shRNA, Mission shRNA	Merck	Cat# TRCN0000003333
Software and algorithms		
Graphpad Prism 9	GraphPad Software	https://www.graphpad.com/company/
GenomicAlignments R package	Bioconductor	https://bioconductor.org/
DESeq2 R package	Bioconductor	https://bioconductor.org/

(*Continued on next page*)

Continued

REAGENT or RESOURCE	SOURCE	IDENTIFIER
Synergy Finder web tool	SynergyFinder	https://doi.org/10.1093/nar/gkaa216
R2 web application	R2: Genomics Analysis and Visualization Platform	http://r2.amc.nl
Other		
Colon cancer spheroid culture medium	Ramesh et al., 2021	DOI: 10.1038/s41418-021-00816-w
Human organoid medium	Ramesh et al., 2021	DOI: 10.1038/s41418-021-00816-w
Human cell line medium	Buikhuisen et al., 2021	doi:10.3390/cancers13040801
4-15% precast gels	Bio-Rad	Cat# 4561084S

RESOURCE AVAILABILITY

Lead contact

Further information and requests for resources and reagents should be directed to and will be fulfilled by the lead contact, Jan Paul Medema (j.p.medema@amsterdamumc.nl)

Materials availability

This study did not generate new unique reagents.

Data and code availability

- RNA-seq data have been deposited at GEO and are publicly available as of the date of publication. Accession numbers are listed in the Key resources table. This paper analyzes existing, publicly available data. Accession numbers for these datasets are listed in the key resources table.
- This paper does not report original code.
- Any additional information required to reanalyze the data reported in this paper is available from the lead contact upon request.

EXPERIMENTAL MODEL AND SUBJECT DETAILS

Spheroid cultures

The colon cancer spheroid culture Co01 (female) was established and transduced with TCF/LEF reporter TOP-GFP as previously described (Vermeulen et al., 2010). Briefly, primary resection from a human colon carcinoma was enzymatically digested with collagenase II (1.5 mg/mL, Sigma-Aldrich) for 1 h at 37°C. Dissociated tissue was then strained through a 70-μm pore, washed, and subsequently cultured. Co01 overexpressing BCL-XL was generated by lentiviral transduction with the pHEFTIR-BCL-XL plasmid as previously described (Colak et al., 2014). Spheroid cultures were cultured in advanced DMEM/F12 (Thermo Fisher Scientific) supplemented with N2 supplement (Thermo Fisher Scientific), 2 mM L-glutamine (Lonza), 0.15% D-glucose (Sigma-Aldrich), 100 μM β-mercaptoethanol (Sigma-Aldrich), trace elements B and C (Thermo Fisher Scientific), 5 mM HEPES (Thermo Fisher Scientific), 2 μg/mL heparin (Sigma-Aldrich), 10 μg/mL insulin (Sigma-Aldrich), epidermal growth factor (Peprotech, EGF, 50 ng/mL), and basic fibroblast growth factor (Tebu-Bio, FGF, 10 ng/mL). Cultures were maintained in ultra-low adherent flasks (Corning) at 37°C and 5% CO_2 and tested for mycoplasma on a monthly basis and confirmed to be mycoplasma negative. Co01 cells were transduced with lentiviral shRNA constructs against either control (SHC002, MISSION shRNA, Merck) or FGFR4 (TRCN0000010531, Mission shRNA, Merck). Transduced cells were selected with 2 μg/mL puromycin (InvivoGen) for 7 days.

Organoid cultures

Patient-derived CRC tumor organoids, P6T (male, 73), P9T (male, 64), P16T (male, 67), and P24aT (female, 60), were obtained from the Clevers organoid biobank and established as previously described (van de Wetering et al., 2015). Normal colon organoids (female, 43) were extracted from a piece of normal mucosa from CRC resection specimens as previously described, at a distance of at least 10 cm from the cancerous tissue (Sato et al., 2011). All experiments on human material are approved by the Medical Ethical Committee of the Academic Medical Center (Amsterdam, the Netherlands) and are in accordance with the Declaration of Helsinki. All human participants provided written informed consent.

Organoids were cultured in drops of growth factor-reduced Matrigel (Corning) in prewarmed 24-well plates. P9T, P16T, and P24aT tumor organoids were maintained in Advanced DMEM/F12 supplemented with N2 and B27 supplement (Thermo Fisher Scientific), antimycotic/antibiotic (Thermo Fisher Scientific), gentamicin (Thermo Fisher Scientific), 2 mM GlutaMax-1 (Thermo Fisher Scientific), 10 mM HEPES, 1 mM *N*-acetyl-L-cysteine (Sigma-Aldrich), 10 nM [Leu15]-gastrin I (Sigma-Aldrich), 10 mM nicotinamide

(Sigma-Aldrich), 500 nM A83-01 (Tocris), 3 μM SB202190 (Sigma-Aldrich), 50 ng/mL human EGF, 20% RSPO1 conditioned medium, 10% Noggin conditioned medium, and 10 nM PGE2 (Santa Cruz Biotechnology). The medium of normal colon organoids was further supplemented with 50% Wnt-conditioned medium and 10 μM ROCK inhibitor (Sigma-Aldrich). P6T was cultured in Advanced DMEM/F12 containing N2 and B27 supplement, gentamycin, 2 mM L-glutamine, 0.15% D-glucose, 100 μM β-mercaptoethanol, trace elements B and C, 5 mM HEPES, 2 μg/mL heparin, 10 μg/mL insulin, 20 ng/mL human EGF, and 10 μM SB202190. Organoids were maintained at 37°C and 5% CO_2 and dissociated every 7–10 days with medium refreshed every 3–4 days. All cultures were confirmed to be mycoplasma negative on a monthly basis.

Cell lines

Adherent colon cancer cell lines HCT116 (male) and SW948 (female) were a kind gift from the Sanger Institute. HCT116 OctaKO cells were kindly provided by the lab of Xu Luo from the University of Nebraska Medical Center (O'Neill et al., 2016). SW948 was maintained as described in Buikhuisen et al., 2021), in 1:1 DMEM/F12 medium containing 15 mM HEPES and 2.5 mM L-glutamine (Gibco) supplemented with 8% fetal bovine serum (Serana) and 50 U/mL of penicillin/streptomycin (Gibco) HCT116 and HCT116 OctaKO cells were maintained in RPMI 1640 medium supplemented with 25 mM HEPES and 2.05 mM L-glutamine (Gibco) supplemented with 8% fetal bovine serum, 1% D-glucose solution plus (Sigma-Aldrich), 1 mM sodium pyruvate (Gibco), and 50 U/mL of penicillin/streptomycin (Buikhuisen et al., 2021). Cultures were tested for mycoplasma contaminations on a monthly basis. HCT116 cells were transduced with lentiviral shRNA constructs against either control (SHC002, MISSION shRNA, Merck) or FGF2 (TRCN0000003333, Mission shRNA, Merck). Transduced cells were selected with 1.5 μg/mL puromycin (InvivoGen) for 7 days.

Mice for platelet toxicity assay

Eight-week-old female NSG mice (Charles River Laboratories) were housed at the University of Palermo in accordance to institutional guidelines of the Italian animal welfare (D.L. n° 26 March 4, 2014) and authorization number 154/2017-PR. Mice (3 per group) were randomly assigned to experiment groups and treated intraperitoneally with a single injection of indicated doses of A-1155463. Platelet counts were evaluated before treatment and at indicated time points using the protocol described in the Method details.

MICE FOR TUMOR GROWTH ASSAY

Six-week-old male NOD/SCID mice (Charles River Laboratories) were housed at the University of Palermo in accordance to institutional guidelines of the Italian animal welfare (D.L. n° 26 March 4, 2014) and authorization number 154/2017-PR. Subcutaneous injection of colon CSCs was performed in the right flank using 300,000 Co01 cells in 100 μL of 1:1 stem cell medium/Matrigel solution. When tumors reached palpable size (0.03–0.06 cm^3), mice were randomized into four treatment groups of four mice each: control, A-1155463 (1 mg/kg), H3B-6527 (5 mg/kg), and A-1155463/H3B-6527 combination. Mice were intraperitoneally treated three times a week for 3 consecutive weeks. Tumors were measured twice per week by a digital caliper. Tumor volume was calculated using the formula: (largest diameter × [smallest diameter]^2)/2. Once the end points were reached (tumor volume = 2 cm^3, or when mice showed signs of suffering), animals were sacrificed accordingly to Directive 2010/63/EU guidelines (D. lgs 26/2016). Platelet counts were evaluated on a weekly basis using the protocol described in the Method details.

METHOD DETAILS

Compounds

The library of 1402 unique inhibitors for high-throughput screening was purchased from Selleck Chemicals (L1100) and includes several small molecule inhibitors, chemotherapeutics and compounds approved by the US Food and Drug Administration. All compounds were dissolved in DMSO and provided at a concentration of 10 mM. A-1155463 (Chemietek) was dissolved in DMSO at 20 mM and WEHI-539 (Selleck Chem) was dissolved in DMSO at 10 mM. Compounds selected from the screen were purchased from Selleck Chemicals and further validated on several cultures for 48 h unless indicated otherwise.

Drug screen workflow

To screen the compounds, Co01 and Co01 BCL-XL were seeded in 96-well flat bottom plates (Corning) at a density of 4000 cells/well. After overnight incubation, cells were treated with the inhibitor library at a final concentration of 1 μM, either alone or in combination with 5 nM A-1155463. All inhibitors were pre-diluted to a concentration of 10 μM in medium and then added to the cells at a further dilution of 1:10 using a dispensing robot. A-1155463 was pre-diluted to a concentration of 50 nM in medium before being robotically dispensed into wells at a 1:10 dilution. Cells were treated for 48 h, after which viability was measured using CellTiter Blue (Promega) as per manufacturer's instructions. Fluorescence readings were measured using the BioTek Synergy HT microplate reader. All drugs were assayed in duplicate on two separate plates and each plate included positive (10 μM A-1155463) and negative controls (DMSO only). Drugs that were toxic on their own at 1 μM were re-tested at a lower dose of 100 nM with and without A-1155463.

Viability assays

Spheroid cultures were seeded in 96-well plates at a density of 4000 cells/well and after overnight incubation, treated with indicated inhibitors in a titration using the HP D300 digital dispenser (Hewlett-Packard) for 48 h. Viability was assessed using CellTiter-Blue following the manufacturer's instructions. Synergy was calculated using the Bliss independence model and scores of greater than 10 were considered synergistic.

Tumor organoids were dissociated from Matrigel in cell recovery solution (BD Biosciences) at 4°C for 30 min. Once the Matrigel was fully dissolved, organoid structures were spun down and trypsinized with TrypLE Express (Thermo Fisher Scientific) for 3 mins at 37 °C. Following dissociation, single cells were washed, counted, and plated in pre-warmed 96-well plates in drops of 6 μL Matrigel at a density of 4000 cells/well. After 3–4 days, organoids were treated in a matrix titration using the HP D300 digital dispenser for 48 h. Viability was assessed using CellTiter-Blue as per the manufacturer's instructions. Synergy was calculated using the Bliss independence model and scores of greater than 10 were considered synergistic.

Normal colon organoids were plated in 48-well plates at approximately 150–300 structures/well. After 3–4 days, organoids were treated with inhibitors for 48 h, after which viability was measured using CellTiter-Blue according to manufacturer's instructions.

Flow cytometry assisted cell sorting

For the caspase assay, Co01 expressing TOP-GFP was plated in 12-well plates at a density of 50,000 cells/well and treated with indicated inhibitors for 24 h. Following treatment, cells were dissociated with Trypsin and stained for activated caspase-3 using RED-DEVD-FMK (CaspGLOW Red, BioVision) as per the manufacturer's instructions.

For FGFR4 staining, cells were resuspended in 0.1% BSA in PBS and incubated with an FGFR4 antibody coupled to PE (clone 4FR6D3, BioLegend) for 30 min on ice, washed, and then measured. Flow cytometry analyses were performed on the FACSCanto II (BD biosciences).

Ex vivo platelet toxicity

Human whole blood was obtained from healthy volunteers in sodium citrate tubes and platelet-rich plasma (PRP) was obtained by centrifugation at 180 rcf for 15 min at room temperature. We pipetted 90 μL of PRP into each well of a 96-well flat bottom plate and treated with indicated inhibitors for indicated time points at 37°C and 5% CO_2. The viability of the platelets was then measured using CellTiter-Blue following the manufacturer's instructions.

Platelet counting from tail vein bleeds

Platelet counts were evaluated before treatment and at indicated time points by collecting tail vein blood in EDTA microvette tubes (Sarstedt). Blood was diluted 1:100 in 1% ammonium oxalate (Sigma-Aldrich) and incubated for 20 min to ensure erythrocyte lysis. We pipetted 10 μL of diluted blood into a hemocytometer and the platelets were allowed to settle before manual counting.

In vivo drug treatment

A-1155463 was first dissolved in DMSO (Sigma-Aldrich) at 80 mg/mL and injected in a solution of 2.75% DMSO, 30% PEG400 (Sigma-Aldrich), 2% Tween-80 (Sigma-Aldrich), and ddH_2O. H3B-6527 was dissolved in DMSO at 20 mg/mL and injected in a solution of 2.75% DMSO, 30% PEG400, 2% Tween-80, and ddH_2O. Control mice received a blank injection of 2.75% DMSO, 30% PEG400, 2% Tween-80, and ddH_2O.

RNA sequencing and data analysis

Total RNA isolation was performed using the Nucleospin RNA isolation kit (Bioke) and duplicate RNA samples of Co01 cells were prepared for RNA sequencing. RNA integrity was assessed using the Agilent 2100 Bioanalyzer (Agilent Technologies). Libraries were prepared using the NEBNext Ultra Directional RNA Library Prep Kit for Illumina as per the manufacturer's instructions and DNA sequencing was performed using the Illumina NextSeq 500 (GenomeScan, Leiden). All reads were mapped to the human genome (GRCh38) using HISAT2. Gene counts (Ensembl build 92) were determined using the summarizeOverlaps function of the GenomicAlignments R package and subsequently normalized to FPKM (fragments per kilobase per million mapped fragments) using the DESeq2 R package. RNA-seq data have been deposited at GEO and are publicly available with accession number GEO: GSE159504. For the gene expression analysis of patient-derived tumor organoids, previously generated data were analyzed using the R2 web application, which is freely available at http://r2.amc.nl (van de Wetering et al., 2015).

Quantitative real-time PCR

Total RNA isolation was performed using the Nucleospin RNA isolation kit (Bioke) and quantified using the NanoDrop 1000 Spectrophotometer (Thermo Fisher Scientific). Synthesis of cDNA was performed using SuperScript III reverse transcriptase (Thermo Fisher Scientific) with random primers (Thermo Fisher Scientific). We used 2× SYBR green master mix (Roche) to perform qRT-PCR as per manufacturer's instructions and FGFR4 (forward: GGAGGAGCCAGGTGAGGA, reverse: CAGGGCTCAAGCTCCACTTC) and FGF2 (forward: TACAACTTCAAGCAGAAGAG, reverse: CAGCTCTTAGCAGACATTGG) transcript levels were measured on the Light Cycler 480 (Roche). RPLP0 (forward: GGCACCATTGAAATCCTGAGTGATGTG, reverse: TTGCGGACACCCTCCAGGAAGC) was used as a housekeeping gene.

Supernatant transfer

Co01 cells were cultured in CSC medium without FGF and treated for 2 h with A-1155463, after which medium was refreshed to wash out the drug. Following another 16 h incubation, supernatants were collected, spun down, and transferred to recipient serum-starved HCT116 or SW948 cells, either with or without H3B-6527 or trametinib (Selleck Chemicals). After 4 h, protein lysates were collected for immunoblot analysis.

Immunoblotting

Following treatment for indicated times, cells were lysed using 1× RIPA Lysis and Extraction buffer (Thermo Fisher Scientific) containing Halt protease and phosphatase inhibitor cocktail (1:100, Thermo Fisher Scientific). Protein samples were quantified using the Pierce BCA protein assay kit (Thermo Fisher Scientific) as per manufacturer's instructions. We loaded 15 μg protein per well into 4%–15% precast gels (Bio-Rad) and then transferred to PVDF membranes using the Trans-Blot Turbo transfer system (Bio-Rad) according to the manufacturer's instructions using the mixed molecular weight transfer settings. Membranes were blocked for 1h in 5% SA in Tris-buffered saline and Tween 20 (TBS-T, 1×) and stained with primary antibody overnight at 4°C. The following primary antibodies were tested: pFGFR4 (1:1000, PA5-37576, Thermo Fisher Scientific) FGFR4 (1:1000, #8562, Cell Signaling), pERK (1:1000, #9101, Cell Signaling), ERK(1:1000, #9107, Cell Signaling), pAKT (1:1000, #4060, Cell Signaling), AKT (1:1000, #9272, Cell Signaling), BCL-XL (1:1000, #2764, Cell Signaling), and MCL-1 (1:1000, #4572, Cell Signaling), phospho-MCL-1 (Thr163, 1:1000, #14765, Cell Signaling) all diluted in 5% BSA in TBS-T. After washing the blots 4 times for 20 min each with TBS-T, the secondary antibody anti-rabbit horseradish peroxidase (1:5000, #4050-05, Southern Biotech) or anti-mouse horseradish peroxidase (1:5000, #1031-05, Southern Biotech) was added for 2 h at room temperature. Following another round of 4 × 20 min washes, the membranes were developed using the LumiLight western blotting substrate (Sigma-Aldrich) and imaged on the ImageQuant LAS4000 (GE Healthcare Life Sciences). GAPDH was used as a loading control (1:5000, MAB374, Sigma-Aldrich).

QUANTIFICATION AND STATISTICAL ANALYSES

All statistical details of experiments can be found in the figure legends. All data in this study are represented as mean ± standard deviation, unless otherwise noted. A two-tailed unpaired Student *t* test was performed to analyze the difference between two independent groups. Ordinary one-way ANOVA was performed to analyze difference between three or more independent groups. *$p \leq 0.05$, ** $p \leq 0.01$, *** $p \leq 0.001$, **** $p \leq 0.0001$. Statistical significance was considered at $p \leq 0.05$. The value of n is provided in each figure legend.

Screen data analysis

Viability data from each screening plate were blank corrected and normalized to control wells. To calculate the effect of combining the drug library inhibitors with A-1155463, replicate values of each drug effect were averaged and subtracted by the average effect of the same drug administered with A-1155463 (Viability $_{drug}$ – Viability $_{drug+A\text{-}1155463}$). This combination effect was calculated for all drugs tested (see Table S1). To eliminate compounds that also affect Co01 BCL-XL, we calculated the difference between the combination effect on Co01 and Co01 BCL-XL and excluded the drugs that had a difference below 20%. Co01 combination effect data were z-score normalized using the formula: *Z* score = (value – mean of all data)/standard deviation of all data. Hits were selected with a *Z* score cut-off of 2 or higher. Assay robustness was measured by the median of the *Z* factor scores calculated for each plate using the formula:

$$Z' = 1 - \frac{3(SD_p + SD_n)}{|Mean_p - Mean_n|},$$

Where *SD* is the standard deviation, *p* is positive control, and *n* is negative control. A score between 0.5 and 1 is indicative of a robust assay (Zhang et al., 1999).

Bliss synergy score

Synergy was calculated using the Synergy Finder web tool (Ianevski et al., 2017) and the Bliss independence model was used to calculate the Bliss score for the most synergistic 3 × 3 dose window in the dose-response matrices. Bliss scores of greater than 10 were considered synergistic.

Cell Reports, Volume *38*

Supplemental information

BCL-XL inhibition induces an FGFR4-mediated rescue response in colorectal cancer

Prashanthi Ramesh, Simone Di Franco, Lidia Atencia Taboada, Le Zhang, Annalisa Nicotra, Giorgio Stassi, and Jan Paul Medema

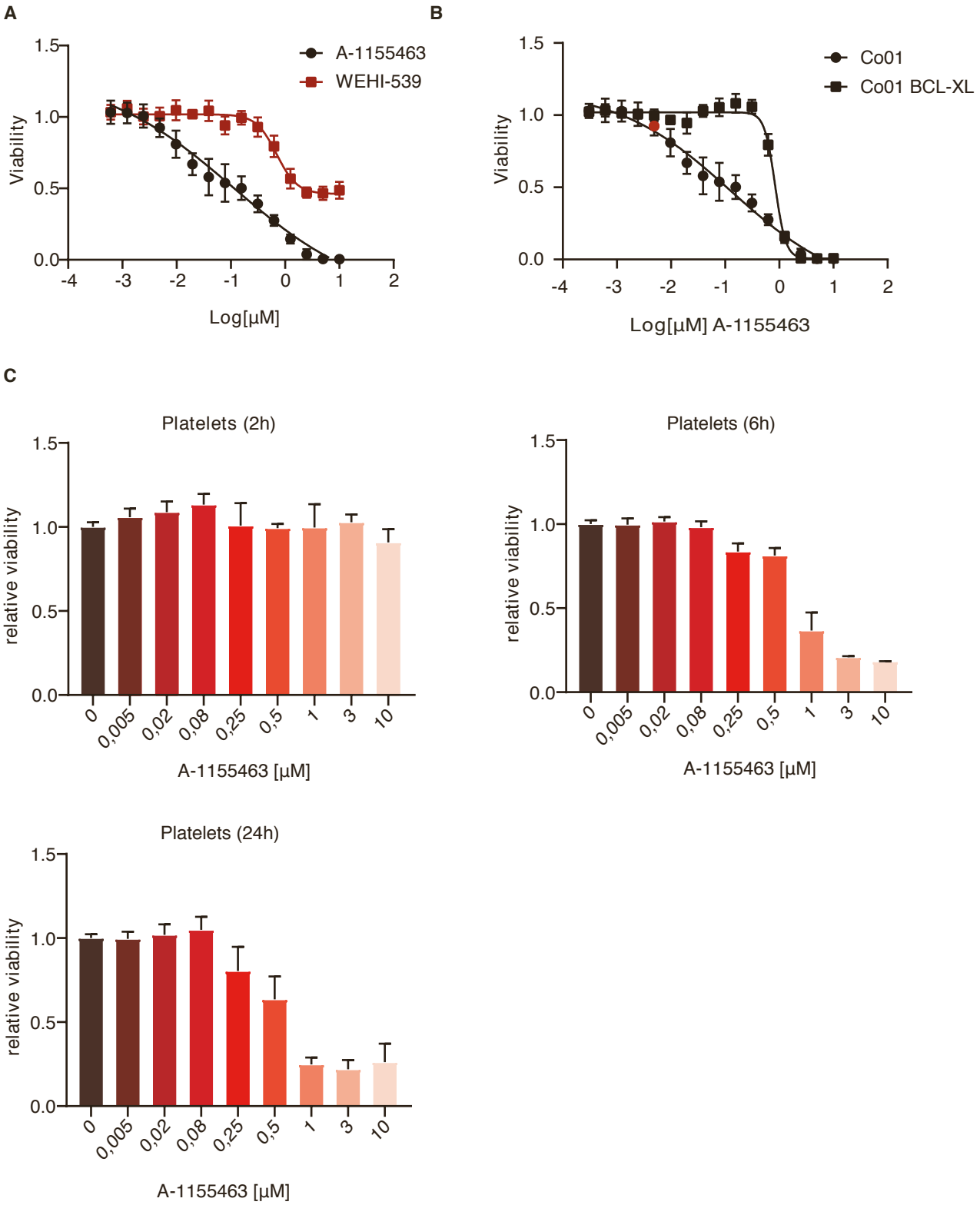

Figure S1. Co01 BCL-XL is resistant to A-1155463, related to Figure 1.
(A) Dose-response curve of Co01 cells treated with a titration of WEHI-539 or A-1155463 for 48 h. Viability data was blank corrected and normalized to control. Data is represented as mean ± SD (n=3 independent experiments).
(B) Dose-response curve of Co01 and Co01 BCL-XL treated with a titration of A-1155463 for 48 h. Viability data was blank corrected and normalized to control. Data is represented as mean ± SD (n=3 independent experiments). The 5nM low dose is highlighted in red.
(C) Viability data of platelets derived from human whole blood treated with increasing doses of A-1155463 for indicated time points. Data represents mean ± SD (n=3 independent experiments).

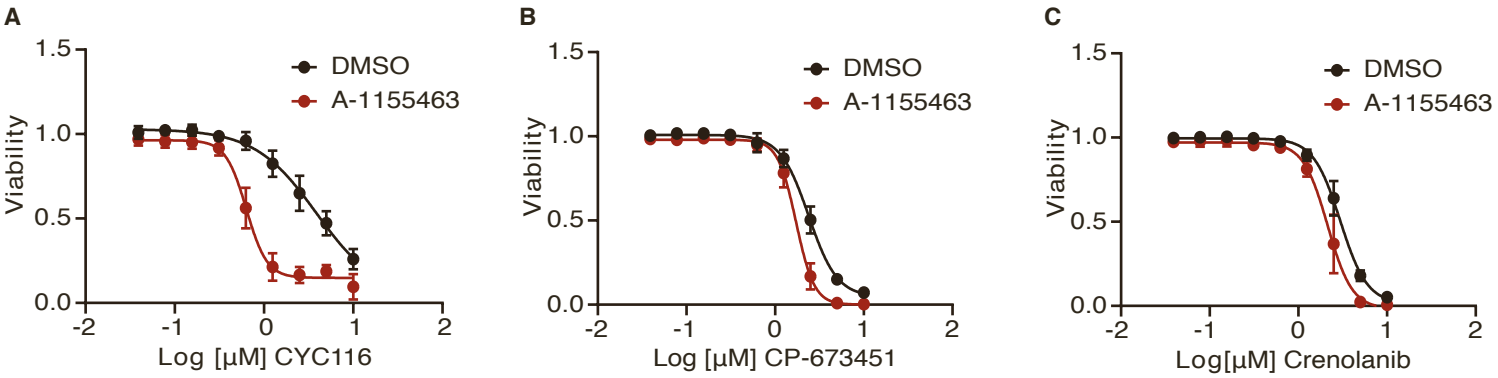

Figure S2. Validation of hits selected from the screen, related to Figure 2.
(A-C) Dose-response curve of Co01 treated with a titration of CYC116 (A), CP-673451 (B) and Crenolanib (C) either alone or in combination with 5nM A-1155463 for 48 h. Viability data was blank corrected and normalized to control. Data is represented as mean ± SD (n=3 independent experiments).

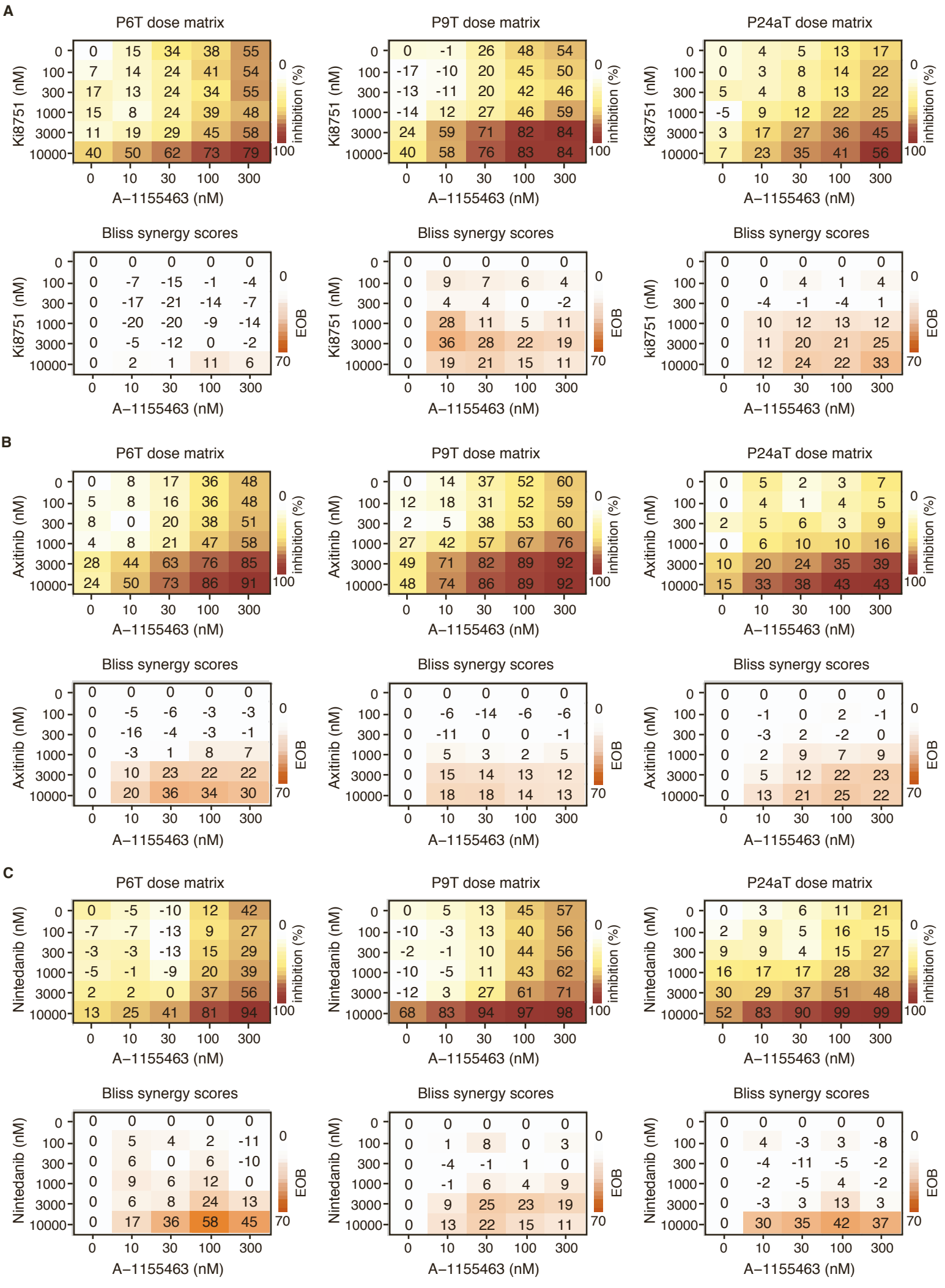
A
P6T dose matrix
P9T dose matrix
P24aT dose matrix
Ki8751 (nM)
A–1155463 (nM)
inhibition (%)
Bliss synergy scores
EOB
B
Axitinib (nM)
C
Nintedanib (nM)

Figure S3. Ki8751, Axitinib and Nintedanib in combination with A-1155463 induce synergistic cytotoxicity in primary patient-derived tumor organoids, related to Figure 3.
(A-C) 5 x 6 dose matrices of P6T, P9T and P24aT human CRC organoids treated with Ki8751 (A), Axitinib (B) and Nintedanib (C) in combination with A-1155463 for 48h. % inhibition was calculated from viability data, after normalizing to control. Data represent the average of three independent experiments. Bliss synergy scores were calculated for each dose combination.

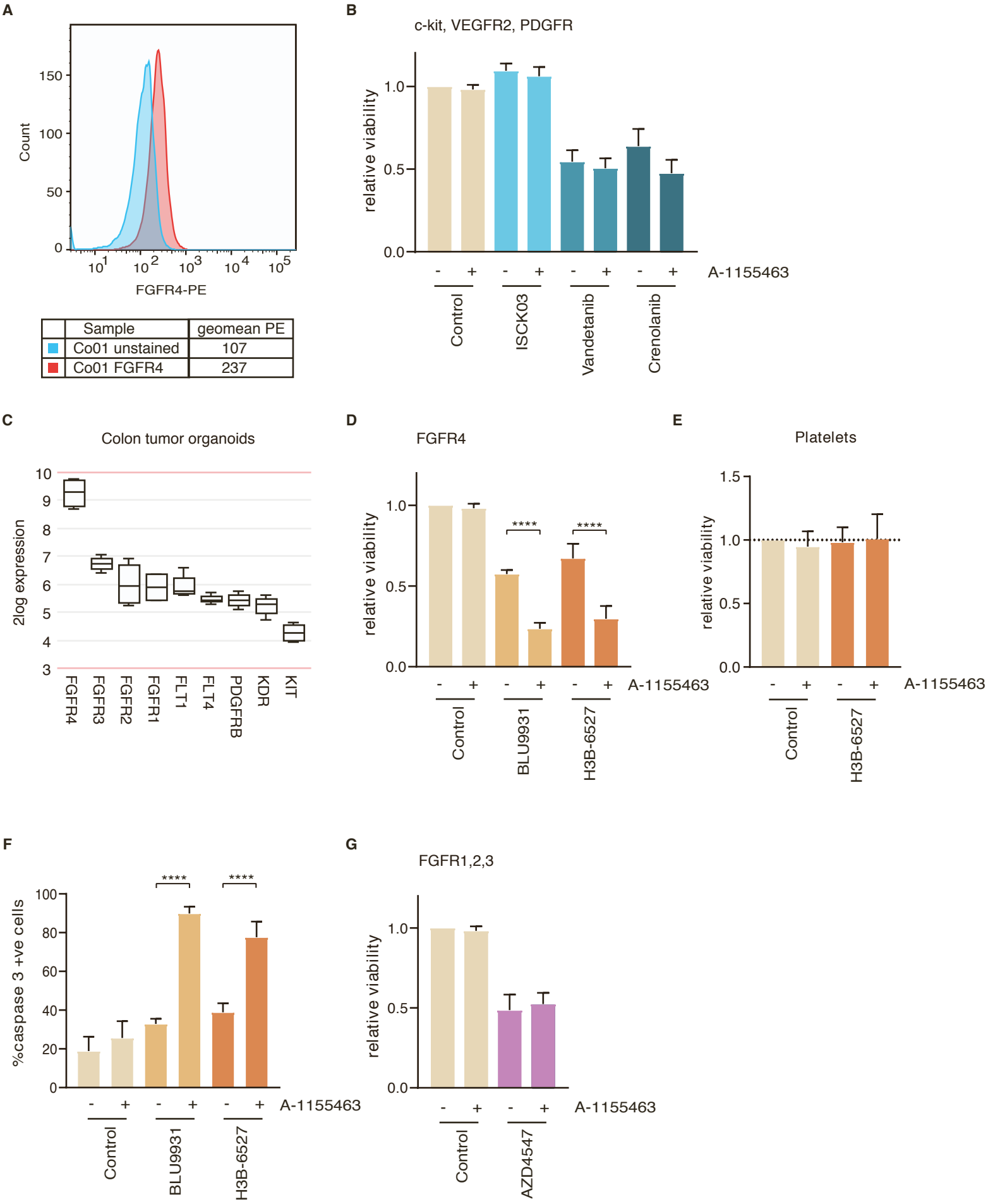
A
Count
FGFR4-PE
Sample
geomean PE
Co01 unstained
107
Co01 FGFR4
237
B
c-kit, VEGFR2, PDGFR
relative viability
A-1155463
Control
ISCK03
Vandetanib
Crenolanib
C
Colon tumor organoids
2log expression
FGFR4
FGFR3
FGFR2
FGFR1
FLT1
FLT4
PDGFRB
KDR
KIT
D
FGFR4
relative viability
****
A-1155463
Control
BLU9931
H3B-6527
E
Platelets
relative viability
A-1155463
Control
H3B-6527
F
%caspase 3 +ve cells
****
A-1155463
Control
BLU9931
H3B-6527
G
FGFR1,2,3
relative viability
A-1155463
Control
AZD4547

Figure S4. FGFR4 inhibition potentiates A-1155463-mediated CSC cell death, related to Figure 4.
(A) Histogram of unstained (blue) and FGFR4 (red) stained Co01 cells analyzed by flow cytometry.
(B) Viability data of Co01 treated with 2.5μM ISCK03, Vandetanib and Crenolanib either alone or in combination with 5nM A-1155463 for 48 h. Cell titer blue measurements were blank corrected and normalized to control. Data is represented as mean ± SD (n=3 independent experiments).
(C) Box plot of mRNA expression levels of known targets of Ki8751, Axitinib and Nintedanib in the patient-derived tumor organoids p6T, p9T, p16T and p24aT.
(D) Viability data of Co01 cells treated with FGFR4 inhibitors BLU9931 and H3B-6527 at 2.5 μM in combination with 5nM A-1155463 for 48h. Cell titer blue measurements were blank corrected and normalized to control. Data is represented as mean ± SD (n=3 independent experiments). ****p value < 0.0001 (two-tailed unpaired Student's t-test).
(E) Viability data of platelets derived from human whole blood treated with 5nM of A-1155463 alone and in combination with 5μM H3B-6527 for 24h. Data is plotted relative to control (dashed line) and represented as mean ± SD (n=3 independent experiments).
(F) Percentage of activated caspase-3 in the 10% TOP-GFP low Co01 cells after 24h treatment with 5μM BLU9931 and H3B-6527, alone and in combination with 5nM A-1155463. Data is represented as mean ± SD (n=3 independent experiments). ****p value < 0.0001 (two-tailed unpaired Student's t-test).
(G) Viability data of Co01 treated with 2.5μM AZD4547 either alone or in combination with 5nM A-1155463 for 48 h. Cell titer blue measurements were blank corrected and normalized to control. Data is represented as mean ± SD (n=3 independent experiments).

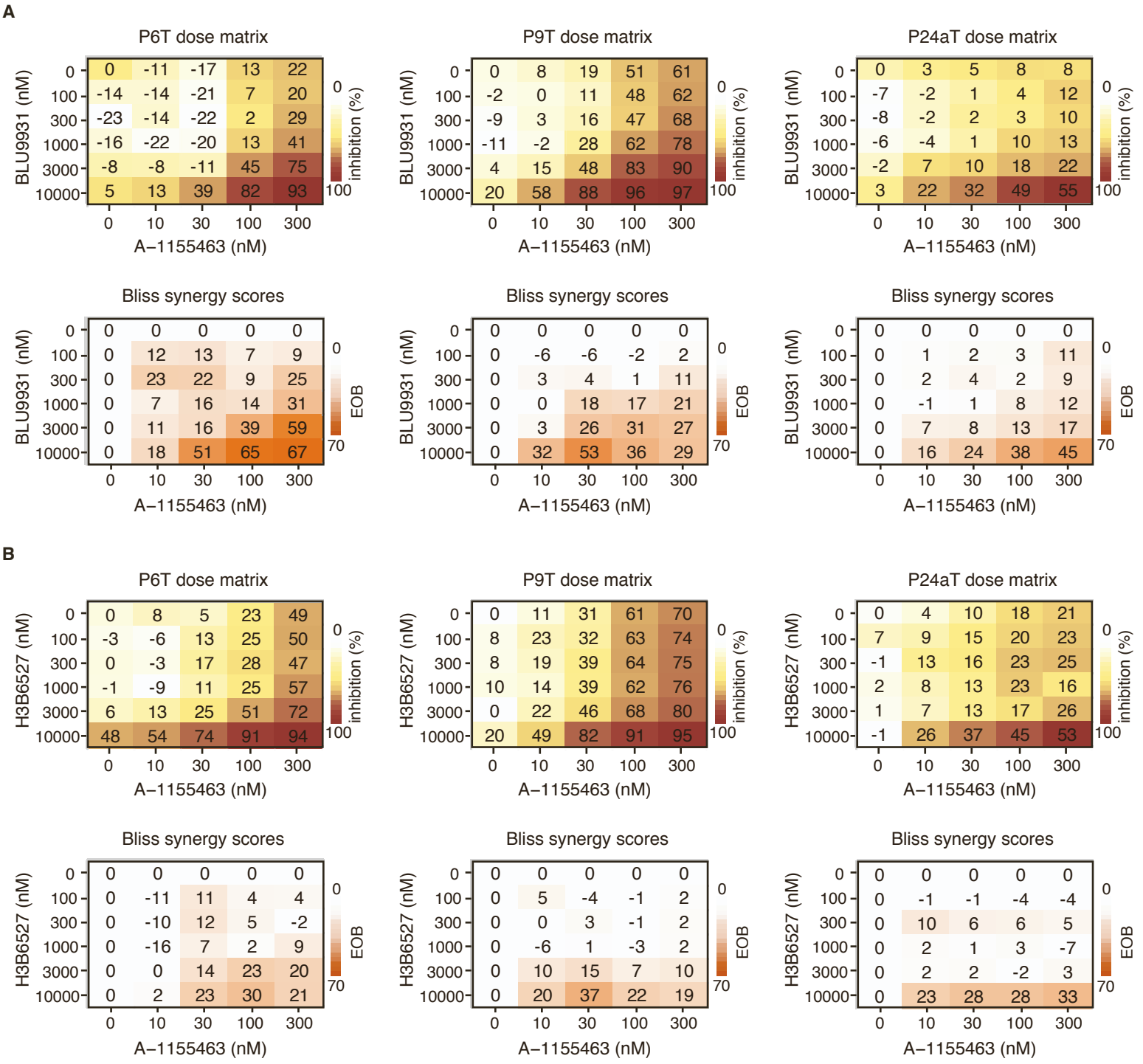

Figure S5. FGFR4 specific inhibitors in combination with A-1155463 induce synergistic cytotoxicity in primary patient-derived tumor organoids, related to Figure 4.

(A, B) 5 x 6 dose matrices of P6T, P9T and P24aT human CRC organoids treated with BLU9931 (A) and H3B-6527 (B) in combination with A-1155463 for 48h. % inhibition was calculated from viability data, after normalizing to control. Data represent the average of three independent experiments. Bliss synergy scores were calculated for each dose combination.

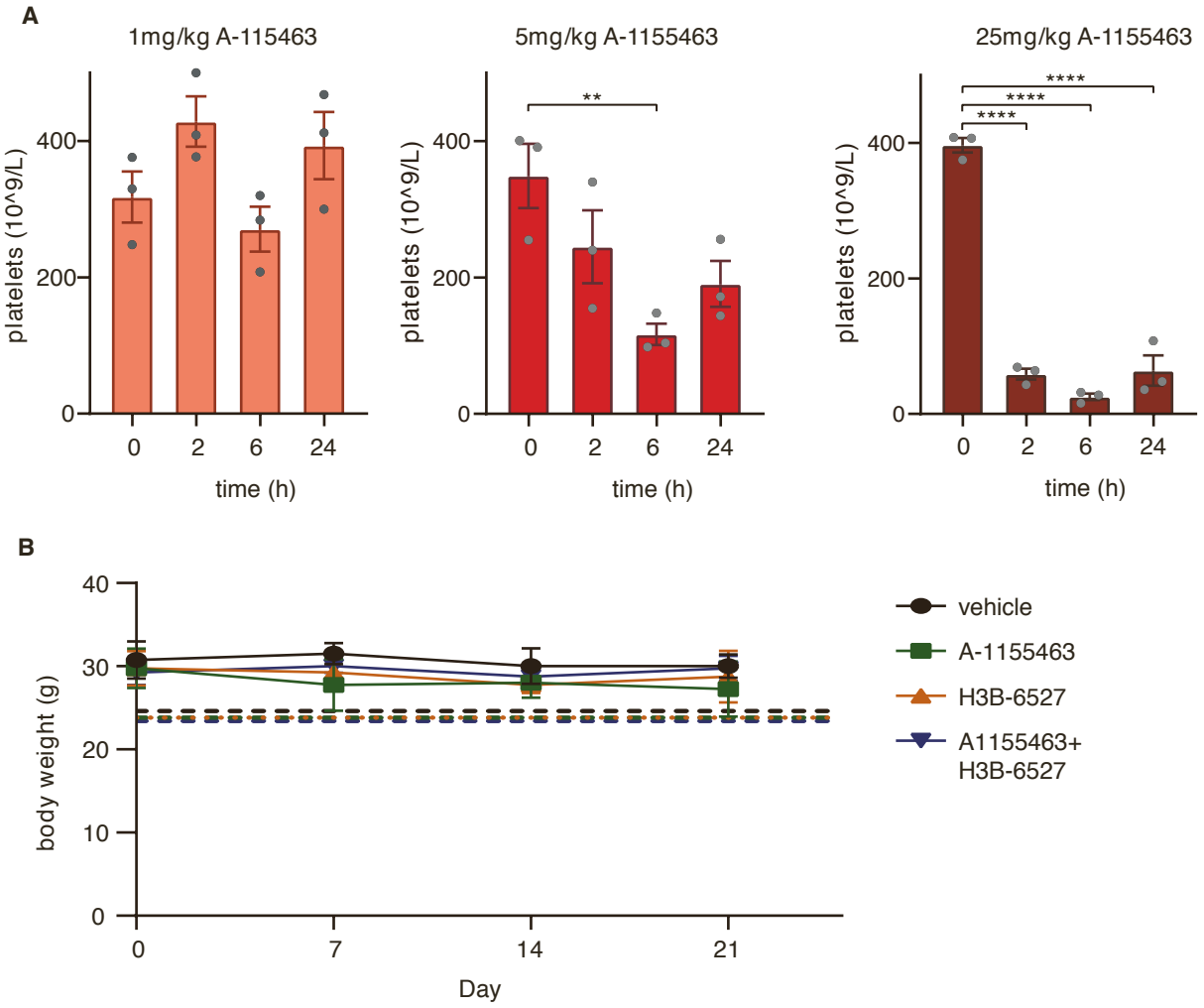

Figure S6. FGFR4 specific inhibitors in combination with A-1155463 induce synergistic cytotoxicity in vivo, related to Figure 4.

(A) Platelet counts determined from tail vein blood of mice treated with a single IP injection of A-1155463 at indicated doses, measured at time 0 before treatment and followed up 2, 6 and 24h after. Data is represented as mean ± SEM (n=3 mice per group). **p value <0.01, ****p value < 0.0001 (Ordinary one-way ANOVA).

(B) Body weight measurements of mice monitored before treatment at day 0 and at the end of each week of treatment at day 7, 14 and 21. Data represents mean ± SD (n=4 mice per group). Dashed lines indicate tolerable amount of weight loss as 20% below weight at day 0 for each treatment group.

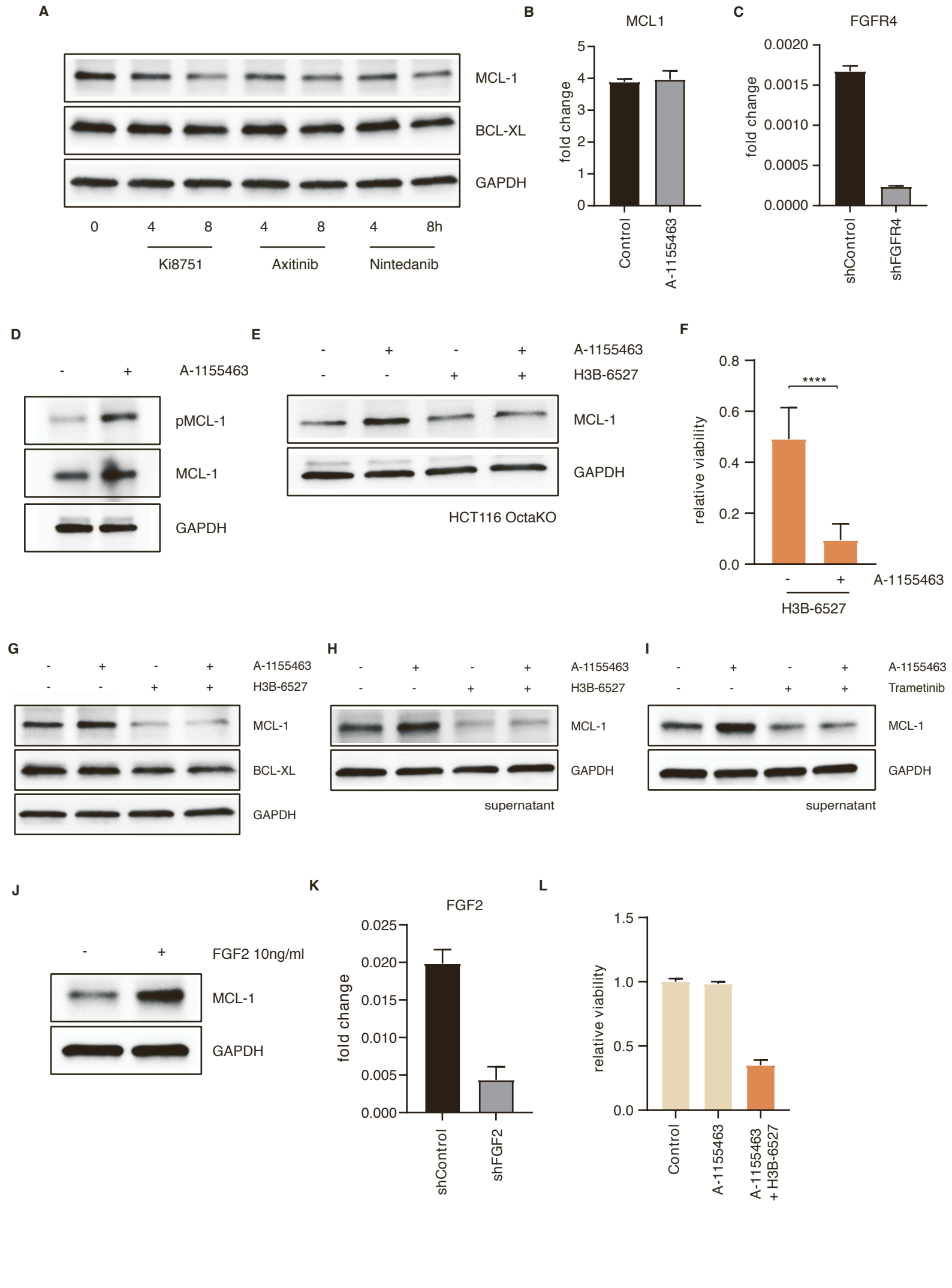
A
MCL-1
BCL-XL
GAPDH
0
4
8
4
8
4
8h
Ki8751
Axitinib
Nintedanib
B
MCL1
fold change
5
4
3
2
1
0
Control
A-1155463
C
FGFR4
fold change
0.0020
0.0015
0.0010
0.0005
0.0000
shControl
shFGFR4
D
-
+
A-1155463
pMCL-1
MCL-1
GAPDH
E
-
+
-
+
A-1155463
-
-
+
+
H3B-6527
MCL-1
GAPDH
HCT116 OctaKO
F
relative viability
0.8
0.6
0.4
0.2
0.0
****
-
+
A-1155463
H3B-6527
G
-
+
-
+
A-1155463
-
-
+
+
H3B-6527
MCL-1
BCL-XL
GAPDH
H
-
+
-
+
A-1155463
-
-
+
+
H3B-6527
MCL-1
GAPDH
supernatant
I
-
+
-
+
A-1155463
-
-
+
+
Trametinib
MCL-1
GAPDH
supernatant
J
-
+
FGF2 10ng/ml
MCL-1
GAPDH
K
FGF2
fold change
0.025
0.020
0.015
0.010
0.005
0.000
shControl
shFGF2
L
relative viability
1.5
1.0
0.5
0.0
Control
A-1155463
A-1155463
+ H3B-6527

Figure S7. BCL-XL inhibition induces an FGFR4-mediated rescue response, related to Figure 5.
(A) Immunoblot analysis of MCL-1 and BCL-XL levels in Co01 cells treated with Ki8751, Axitinib and Nintedanib at 1μM for several time points. GAPDH was used as a loading control.
(B) qRT-PCR analysis of MCL1 expression levels in Co01 cells treated with 5nM A-1155463 for 24h. Data is represented as mean ± SD (n=3).
(C) qRT-PCR analysis of FGFR4 expression levels in Co01 cells transduced with shControl or shFGFR4 to confirm effective knockdown.
(D) Immunoblot analysis of pMCL-1 and MCL-1 in HCT116 cells treated with 10nM A-1155463 for 2h. GAPDH was used as a loading control.
(E) Immunoblot analysis of MCL-1 levels in HCT116 OctaKO cells treated with 500nM A-1155463, 5μM H3B-6527 or a combination of the two for 4h. GAPDH was used as a loading control. Blots represent one of two independent experiments with similar results.
(F) Viability data of Co01 cells treated with H3B-6527 at 5μM in combination with 5nM A-1155463 for 48h, without bFGF in the culture medium. Cell titer blue measurements were blank corrected and normalized to control. Data is represented as mean ± SD (n=2 independent experiments). ****p value < 0.0001 (two-tailed unpaired Student's t-test).
(G) Immunoblot analysis of MCL-1 and BCL-XL levels in Co01 cells cultured in medium without bFGF, treated with 5nM A-1155463, 5μM H3B-6527 or a combination of the two for 4h. GAPDH was used as a loading control.
(H) Immunoblot analysis of MCL-1 levels in SW948 cells that received supernatant of control or 5nM A-1155463 conditioned cells as described in Figure 5F, in the presence or absence of 5μM H3B-6527 for 4h. GAPDH was used as a loading control.
(I) Immunoblot analysis of MCL-1 levels in SW948 cells that received supernatant of control or 5nM A-1155463 conditioned cells as described in Figure 5F, in the presence or absence of 5μM Trametinib for 4h. GAPDH was used as a loading control.
(J) Immunoblot analysis of MCL-1 levels in SW948 cells treated with 10ng/ml FGF2 for 4h. GAPDH was used as a loading control.
(K) qRT-PCR analysis of FGF2 expression levels in HCT116 cells transduced with shControl or shFGF2 to confirm effective knockdown.
(L) Viability data of Co01 cells treated with 1nM A-1155463 in combination with 5μM H3B-6527 for 48h. Cell titer blue measurements were blank corrected and normalized to control. Data is represented as mean ± SD (n=3 independent experiments).
All blots represent one of two independent experiments with similar results.